Oncogenic KRAS cells use Wnt signalling and cell dormancy to override homeostatic cell elimination mechanisms in adult pancreas.

Beatriz Salvador-Barbero[1], Markella Alatsatianos[1], Jennifer P. Morton[2, 3], Owen J. Sansom[2, 3], Catherine Hogan[1]*.

1. European Cancer Stem Cell Research Institute, School of Biosciences, Cardiff University, Cardiff CF24 4HQ, UK.
2. CRUK Scotland Institute, Glasgow, G61 1BD, UK.
3. School of Cancer Sciences, University of Glasgow, Glasgow, G61 1QH, UK.

*Correspondence to hoganc@cardiff.ac.uk

Abstract

Epithelial tissues use homeostatic defence mechanisms to actively remove aberrant or poorly functioning cells to maintain tissue health. We show that when present in tissues in low numbers, cells expressing cancer-causing mutations compete with normal cells for survival and are often eliminated. This implies that tumour initiation would require mechanisms whereby mutant cells override tissue homeostasis and remain in a tissue; however, the biology of these initial events is poorly understood. Here, we use an *in vivo* model of sporadic tumorigenesis in the adult pancreas to show that cell elimination processes are inefficient and a proportion of KrasG12D or p53R172H expressing cells are never eliminated from the epithelium. Using RNA sequencing of non-eliminated mutant populations, we reveal a general activation of the non-canonical Wnt pathway. We demonstrate that non-eliminated KrasG12D cells express cell dormancy and diapause gene signatures, suggesting non-eliminated KRasG12D cells adopt a dormant cell state *in vivo*. To model cell competition *in vitro*, we used established MDCK cell systems to show that active Wnt or cell cycle arrest blocks elimination of RAS mutant cells from normal epithelial cell sheets. Importantly, we demonstrate that Wnt signalling is a general mechanism that blocks elimination of some KrasG12D and p53R172H cells from pancreas tissues *in vivo*. Our results suggest that mutant cells activate Wnt and/or a dormant cell state to avoid homeostatic tissue defence mechanisms and survive in the adult pancreas.

Keywords: Epithelial homeostasis, cell elimination, cell competition, Kras, mutant p53, pancreas, Wnt, cell dormancy, pancreatic cancer.

Introduction

Epithelial tissues are continuously exposed to mutational insults, and as a result, genetically mutant cells often arise in a tissue. Indeed, most human cancers start sporadically from epithelial cells carrying genetic mutations that activate oncogenes or inactivate tumour suppressor function. Remarkably, epithelial tissues protect against tumorigenesis by actively removing aberrant (*1, 2*) and genetically mutant cells (*3-9*). In general, genetically different cells compete for space and survival in tissues, resulting in the elimination of 'less fit' mutant cells via apoptosis, extrusion and/or cell differentiation (*10*). Cell competition outcomes are dependent on the genetic status of a cell relative to its local neighbourhood (*10, 11*) and extrinsic environmental factors (*12-14*) and therefore under certain conditions, competition is tipped in favour of mutant cells. This is better understood in rapidly proliferating tissues that are actively replenished via defined stem cell compartments; tumour risk increases when stem cells acquire genetic mutations that confer a competitive advantage over wild type counterparts, allowing the mutant stem cells to completely occupy the niche (*15-18*). In contrast, our understanding of how cell competition outcomes shape tumorigenesis in slow proliferating adult tissues that lack a *bona fide* stem cell compartment remains poorly detailed.

Using mouse pancreas as a model system of a slow proliferating adult tissue, we recently demonstrated that cells expressing oncogenic *Kras* (*Kras*^{G12D}) are outcompeted by healthy neighbours and are eliminated from exocrine and endocrine epithelial compartments (*4*). We have previously described how interactions with normal cells trigger robust evolutionary conserved cell biology phenotypes in *Ras* transformed cells, resulting in the elimination of the mutant cells via cell segregation and cell extrusion (*4, 5, 9, 19*). Removal of KrasG12D cells from adult pancreas tissues requires local remodelling of E-cadherin-based cell-cell adhesions at normal-mutant boundaries and dynamic changes in mutant and normal cell volume (*4*). Importantly, we demonstrated that abrogation of KrasG12D cell elimination in the pancreas significantly increased the appearance of preneoplastic lesions (*4*), suggesting cell competition and cell elimination are disease preventative.

Activating mutations in oncogenic *RAS* are the principal driver gene event in human pancreatic ductal adenocarcinoma (PDAC; (*20*)), the most common type of human pancreatic cancer. *KRAS* mutations are detected in >90% of human tumours and *in vivo* mouse studies show that KRAS signalling is essential for disease to progress through all stages (*21*). Missense mutations in *TP53* are the second most common mutation detected in ~70% of human PDAC (*22*) and required for metastasis (*23*). How genetically mutant cells survive and grow in the competitive environment of the adult pancreas remains unclear. Here, we sought to understand the mechanisms underpinning how mutant cells avoid elimination and survive in the adult pancreas. Using *in vivo* models of sporadic

tumorigenesis, we confirm that adult pancreas tissues actively eliminate cells expressing either oncogenic KrasG12D or p53R172H mutations; however, some mutant cells are never eliminated, suggesting these cells have a competitive advantage. We report that cell competition is completely abrogated when tissues contain ‘double mutant’ cells, i.e., cells expressing both KrasG12D and p53R172H mutations. Using bulk RNA sequencing, we identify gene signatures of ‘never-eliminated’ mutant cells. Using cell competition assays *in vitro* and *in vivo*, we demonstrate a functional role of Wnt signalling as an important general regulator of mutant cell fate and cell dormancy as a second mechanism, whereby KrasG12D cells avoid cell elimination.

Results

Cells expressing p53R172H mutations are outcompeted and eliminated from adult pancreas compartments. Cells co-expressing p53172H and KrasG12D mutations are never eliminated.

To model sporadic pancreatic cancer, we used the pancreas-specific genetically engineered mouse models: KC: *Pdx1-Cre^{ERT}; LSL-Kras$^{G12D/+}$; Rosa26$^{LSL\text{-}tdRFP}$*; PC: *Pdx1-Cre^{ERT}; LSL-Trp53$^{R172H/+}$; Rosa26$^{LSL\text{-}tdRFP}$*; and KPC: *Pdx1-Cre^{ERT}; LSL-Kras$^{G12D/+}$; Trp53$^{R172H/+}$; Rosa26$^{LSL\text{-}tdRFP}$*. Our experimental control was *Pdx1-Cre^{ERT}; Rosa26$^{LSL\text{-}tdRFP}$* mice (Fig. 1A left). Adult mice were treated with low-dose tamoxifen to induce transgene expression (together with RFP reporter) in a mosaic manner in all pancreatic epithelial compartments (*4*). To monitor genetically mutant cell fate, we measured RFP levels in tissues harvested at 7-, 35- and 70-days post induction (p.i.) of Cre recombinase (Fig. 1A-1C). Consistent with our previously published data (*4*), we found that low dose tamoxifen induced stochastic RFP labelling in ~20-25% of the tissue (Fig. 1C); levels of RFP fluorescence were comparable between all genotypes at 7 days (Fig. 1B, top panels; 1C; (*4*)) and significantly decreased over time in KrasG12D tissues (KC; Fig. 1B, lower panel; 1C, $p<0.0001$ for both 35 and 70 days p.i.). RFP fluorescence also significantly decreased over time in tissues expressing p53R172H mutations (PC; Fig. 1B, lower panel; 1C, $p<0.0001$ and $p=0.0173$ at 35 and 70 days p.i. respectively). In contrast, we found no significant difference in the level of RFP in double mutant (KPC) tissues over time (Fig. 1B, lower panel; 1C, p=0.2062 and p=0.1504 at 35 and 70 days p.i. respectively). RFP+ ducts were significantly less frequent in KrasG12D (KC) and p53R172H (PC) tissues at the 7-day p.i time point, compared to controls (Fig. 1D, $p=0.0038$ and $p=0.0029$ respectively), while the number of RFP+ ducts in double mutant (KPC) tissues was comparable to controls (Fig. 1D, $p=0.2879$). We also measured a significant decrease in the percentage of RFP+ cells per islet in p53R172H (PC) and KrasG12D (KC) tissues (Fig. 1E, $p=0.0214$ and $p=0.0134$ respectively), whereas the frequency of RFP+ cells per islet in double mutant (KPC) tissues was also comparable to wild type controls (Fig. 1E, $p=0.5394$). Thus, like KrasG12D-expressing cells (*4*), p53R172H single mutant cells are eliminated from all epithelial compartments. Cells expressing both KrasG12D and p53R172H mutations are never eliminated from endocrine/exocrine epithelial tissues.

We have previously shown that KrasG12D cells are competitively eliminated at cell boundaries with surrounding normal cells, resulting in the elimination of small clusters (*4, 24*). Similar to our previously published results (*4*), the percentage of small clusters (<50 micron^2) significantly decreased in KrasG12D (KC; Fig. 1F, $p=0.0004$) and in p53R172H (PC; Fig. 1F, $p=0.0316$) tissues over time. We did not see significant differences in cluster distribution based on size in double mutant (KPC) tissues, compared to controls (Fig. 1F; $p=0.7740$, small clusters), suggesting double mutant (KPC) cells do not respond to cell-cell

interactions with normal cells. Thus, expression of p53R172H mutations in low numbers of cells in adult pancreas tissues triggers cell competition *in vivo*, resulting in elimination of p53R172H cells. Co-expression of mutant p53R172H confers a survival advantage to KrasG12D cells, abrogating competition in the tissue and allowing KrasG12D cells to avoid cell elimination.

Transcriptional profiles of non-eliminated mutant cells indicate activation of pro-survival signals.

We consistently found that ~10% of tissue area remains RFP-labelled in KrasG12D (KC) and in p53R172H (PC) tissues post the 35-day time-point (Fig. 1B, 1C; (*4*)), indicating that some mutant cells are never eliminated from the pancreas *in vivo*. Consistent with our previously published report (*4*), we found rare Alcian blue positive lesions (SFig. 1A, left panels) in 6/9 KrasG12D (KC) mice at 168 days p.i., suggesting some non-eliminated KrasG12D cells progress to pancreatic intraepithelial neoplasia (PanINs) (*25*). We did not detect PanIN lesions in p53R172H (PC) tissues. As expected, PanIN lesions were detected more frequently in 5/5 KPC tissues analysed (SFig. 1A, right panel) and 4/5 mice developed PDAC tumours by 168 days p.i.

We hypothesised that non-eliminated mutant cells override competitive cell elimination signals via common mechanisms. A deeper understanding of how KrasG12D cells avoid cell elimination may inform on the biology of early tumorigenesis. To gain an unbiased insight into how non-eliminated mutant cells survive in tissues we performed bulk RNA sequencing (Fig. 2A). Whole pancreata were harvested from experimental cohorts (KC/PC/KPC/Control) at 35 days p.i. and digested to cell suspensions. We used anti-lectin antibodies to enrich for acinar/ductal epithelial cells, as it is generally accepted that PDAC originates from genetically mutant acinar and/or ductal epithelial cells (*26*), and FACS sorted leptin positive RFP positive cells. To ensure we reached a minimum of 5,000 viable lectin positive RFP positive cells per sample, we pooled cell suspensions generated from three pancreas tissues per genotype. This was repeated to generate three samples per genotype for sequencing. We compared differential gene expression in non-eliminated mutant cells to wild type controls and found that KrasG12D cells (KC) predominantly upregulated genes, while p53R172H (PC) and double mutant (KrasG12D p53R172H, KPC) cells downregulated genes (Suppl. Table S1, S2). We found few differentially expressed genes in common between non-eliminated mutant cells when compared to wild type control (see Suppl. Table S1-S3).

To elucidate the biological pathways underpinning mutant cell retention in pancreas tissues, we applied gene set enrichment analysis (GSEA_4.2.2; entire Hallmarks and KEGG MEDICUS databases) and compared non-eliminated KrasG12D (KC) or p53R172H (PC)

transcriptomes to wild type controls. We found that KrasG12D (KC) signatures positively correlated with MAPK (Fig. 2B, SFig. 2A) and p53 (Fig. 2B, SFig. 2B) signalling pathways, compared to controls, whereas p53R172H (PC) signatures negatively correlated with p53 (Fig. 2C, SFig. 2C) and with Kras (Fig. 2C) and MAPK (SFig. 2D) signalling. Non-eliminated KPC signatures also downregulated KRAS signalling (SFig. 2E), suggesting deregulation of Kras signalling and/or p53 pathway is a general requirement for mutant cells to remain in tissues. We found that KrasG12D (KC) signatures positively enriched for pathways associated with stress responses (Fig. 2B, e.g., Oxidative phosphorylation, Hypoxia, Unfolded protein response, UV response), deregulation of cell cycle (e.g., E2F targets and G2/M checkpoint) and immune response (e.g., Il2-Stat5 signalling, TNFa via NFkB signalling). In contrast, pathways associated with p53, cell cycle and inflammatory responses were negatively enriched in p53R172H (PC) signatures (Fig. 2C). Notably, KrasG12D (KC) signatures positively enriched for pro-survival and pro-tumorigenic pathways (Fig. 2B, e.g., Epithelial to Mesenchymal Transition (EMT), TNF-α signalling, Hypoxia, Angiogenesis, Notch signalling, Wnt signalling). Gene signatures from both p53R172H (PC; Fig. 2C) and KrasG12D p53R172H (KPC; SFig. 2E) negatively enriched for apoptosis, suggesting cell survival is also a requisite for mutant cell retention in tissues.

Gene signatures of non-eliminated KrasG12D cells correlate with PDAC initiation and with increased stemness and cellular reprogramming.

Mouse models of pancreatic cancer show that expression of oncogenic *Kras* triggers injury and stress responses, which often translate as cellular reprogramming and a change in cell fate (*27*). We found that KrasG12D (KC) gene signatures positively correlated with WP_Pancreatic_Adenocarcinoma_Pathway in GSEA analysis (SFig. 2F). Consistent with GSEA analyses, we found that gene signatures of non-eliminated PC (p53R172H) and KPC (KrasG12D p53R172H) cells negatively correlated with pro-tumorigenic pathways (Fig. 2C, SFig. 2E, 2G, 2H). Using published datasets (*27*), we screened transcriptomes of non-eliminated cells and found canonical markers of spasmolytic polypeptide-expressing metaplasia (SPEM (*28*); e.g., *Aqp5, Tff2, Dmbt1, Gkn3, Wfdc2*) were upregulated in non-eliminated KrasG12D (KC) cells (SFig. 2I). We also found upregulation of acinar genes (e.g., *Ptf1a, Rbpjl*), ductal genes (e.g., *Sox9, Onecut1*) and mucin genes (e.g., *Muc5a*, *Spdef, Creb3l4, Creb3l1*) in non-eliminated KrasG12D (KC) cells (SFig. 2J). Finally, we found stemness gene signatures enriched in KrasG12D cells (Ramalho_stemness_up (M9473) and Malta_curated_stemness_markers (M30411) GSEA gene sets; KC) compared with control (SFig. 2K, 2L). We did not see enrichment of these gene signatures in p53R172H-expressing populations (SFig. 2I, 2J, 2M, 2N). We consistently showed that ductal epithelial compartments efficiently eliminate mutant cells and very few RFP+ cells remain in ducts at

35 days p.i. cells (Fig. 1D; (*4*)). Thus, we assume that most RFP+ cells isolated for RNA sequencing are acinar in origin. Our gene signature data imply that non-eliminated KrasG12D populations represent differentiated acinar cells and early embryonic pancreatic progenitors, cells undergoing acinar-ductal metaplasia, gastric pyloric and intestinal metaplasia. The data also demonstrate that canonical KrasG12D-induced disease-associated metaplasia is evident in tissues at very early time points (35 days post activation of the transgene).

Non-eliminated KrasG12D mutant cells express features of cell dormancy.

Several of our data indicated that non-eliminated cells are not actively dividing in tissues over time, e.g., we found no change in the amount of RFP fluorescence in tissues over time (Fig. 1C), suggesting RFP+ cells are not expanding. Consistently (*4*), immunostaining for Ki-67 showed an absence of proliferation in all tissues (Fig. 3A). GSEA analyses identified enrichment of proliferation-related pathways (e.g., E2F targets, GF-Rtk-Ras-Erk signalling) in non-eliminated KrasG12D cells compared to controls (KC; Fig. 2B); however, analysis of specific gene signature data showed a general downregulation of cell cycle genes (KC; Fig. 3B). GSEA analysis also revealed enrichment of pathways indicative of dysregulation of the cell cycle towards genomic instability (*29, 30*) (Fig. 2B, e.g., G2M checkpoint, Htlv Tax to spindle assembly checkpoint, Hbv-Hbx to Ras/Erk signalling, DNA-replication termination). Cell cycle gene expression profiles of non-eliminated p53R17H cells compared to wild type controls (PC; Fig. 3B) was similar to that of KrasG12D signatures. GSEA analyses indicated a general downregulation of proliferation-related pathways (e.g., E2F targets, Myc targets, Kras signalling up) in mutant p53-expressing cells (PC; Fig. 2C; KPC; SFig. 2E). Using β-galactosidase as a readout, we found no evidence of cell senescence in 35-day KrasG12D (KC) pancreas tissues (SFig. 3A). We also counted rare caspase-3 positive events in all pancreas tissues analysed (Fig. 3C), suggesting a general absence of apoptosis. We hypothesised that non-eliminated cells deregulate and/or arrest in the cell cycle. Indeed, non-eliminated KrasG12D (KC) gene signatures were also enriched for pathways associated with cancer cell dormancy, (e.g., Oxidative phosphorylation, Unfolded protein response, Hypoxia, Fig. 2B) (*31*). In general, cell dormancy describes a reversible cell cycle arrested state, often triggered by cell stress (*32-34*). Using published gene signatures of cell dormancy as reference (*35*), we found cell dormancy (Fig. 3D) and diapause (SFig. 3B) gene signatures are enriched in non-eliminated KrasG12D (KC) cells compared to control cells. Diapause is a temporary halt in embryogenesis when conditions are detrimental to development (*34*). We also found NRF2 pathway (SFig. 3C) and NRF2 target genes (SFig. 3D) were positively enriched in non-eliminated KrasG12D (KC) cells. NRF2 is a transcription factor, which is activated during cell dormancy (*36*). Cell dormancy/diapause gene

signatures or related pathways were not significantly enriched in non-eliminated p53R172H (PC) cells (Fig 3D, SFig. 3B). These data infer that non-eliminated mutant cells deregulate the cell cycle towards a cell cycle arrested state; however, two copies of functional p53 are required for cells to adopt a dormant or diapaused state (*37-39*).

Cell cycle arrest prevents cell elimination *in vitro*.

We hypothesised that mutant cells override cell elimination by arresting in the cell cycle. To functionally test this, we used previously established cell competition assays and Madin-Darby Canine Kidney (MDCK) cells expressing GFP-tagged constitutively active oncogenic RasV12 (GFP-RasV12) (*5, 9*). We have previously shown that when surrounded by normal MDCK cells, GFP-RasV12-expressing MDCK cells are outcompeted and eliminated from an epithelial sheet via cell extrusion (*5, 9*). Once extruded, GFP-RasV12 cells rapidly proliferate to form multicellular aggregates (*5*). In contrast, MDCK cells expressing mutant p53 (p53R175H, p53R273H) are outcompeted by normal cells via necroptosis (*40*). We induced cell cycle arrest in GFP-RasV12 cells via *Myc* knockdown and transient transfection of two independent c-Myc siRNAs (transfected alone or in combination; siMyc-GFP-RasV12). We chose *c-Myc* knockdown as an approach because c-Myc is a key regulator of the cell cycle (*41*) and depletion of Myc triggers cell dormancy (*42*). Expression of c-Myc siRNA yielded a decrease in MYC protein levels, 48h post-transfection (SFig. 3E, 3F), an increase in p21 protein expression and decreased phospho-p38 protein levels (SFig. 3E, 3F) and a marked reduction in GFP-RasV12 cell confluency (SFig. 3G) compared to GFP-RasV12 cells expressing scrambled siRNA controls (siScr-GFP-RasV12). Thus, transient depletion of Myc in GFP-RasV12 cells promotes cell cycle arrest. To assess the impact of cell cycle arrest on normal-mutant cell-cell interactions, we used our established cell extrusion assay (*5, 9*), whereby GFP-RasV12 cells were first transfected with siScr or siMyc oligos and then mixed with normal MDCK cells at 1:50 ratios. At 48h post mixing, cells were fixed, stained with phalloidin and Hoechst to visualise F-actin and nuclei respectively. We scored cell extrusion events and found that the proportion of non-extruded GFP-RasV12 cells significantly increased when GFP-RasV12 cells were depleted for MYC (siMyc-GFP-RasV12; Fig. 3E, 3F; p=0.0003 siMyc1+2-GFP-RasV12 compared to siScr-GFP-RasV12 controls). Immunofluorescence staining using anti-Ki-67 antibodies confirmed that non-extruded siMyc-GFP-RasV12 cells are not proliferating, whereas the minority of Ki-67 positive cells were extruded (Fig. 3G, 3H). We also used cell confrontation assays (*9*) and live-cell imaging of normal-mutant interactions across an entire epithelial cell sheet (SFig. 3H). We previously reported that upon collision with normal MDCK cells, GFP-RasV12 cells are triggered to retract and segregate away from normal cells, separating via the formation of smooth boundaries (*9*). We found that GFP-RasV12 cells depleted for MYC (siMyc1+2) retracted

less efficiently than GFP-RasV12 siScr controls (SFig. 3I, SFig.3J; *p*=0.0086). Thus, RasV12 cells depleted for Myc and exhibiting cell cycle arrest are not extruded or triggered to segregate by normal cells, suggesting cell cycle arrest protects RasV12 mutant cells from cell elimination.

Active Wnt signalling prevents KrasG12D cell extrusion *in vitro*.

The Wnt pathway positively regulates cancer cell dormancy (*43, 44*), diapause (*31*) and stemness (*45, 46*) in different tissue contexts. GSEA analyses identified an enrichment for Wnt pathway activation in KrasG12D (KC) transcriptomes compared to controls (Fig. 2B; Wnt signalling modulation Lgr/Rspo, Wnt5a-Ror signalling pathway). Gene expression data identified increased expression of both Wnt target genes and components of the Wnt pathway such as ligands and receptors (Fig. 4A). Genes commonly associated with the Wnt/β-catenin pathway and induction of cell stemness/proliferation, were generally downregulated in KrasG12D (KC) cells, including *Lgr5*, *Myc*, *Sox2*, *Nanog*, *Esrrb* and *Wnt3a* (Fig. 4A, 4B). Conversely, expression of Wnt ligands and receptors associated with activation of β-catenin independent Wnt signalling were increased in KrasG12D (KC) cells, including *Wnt4*, *Wnt5a*, *Ror1* and *Ror2*, and the transcription factor *Jun* (Fig. 4A and Supplementary table S11). Indeed, *Wnt5a* expression was increased at the mRNA level in non-eliminated KrasG12D (KC) cells (Fig. 4C). GSEA analyses indicates low levels of Wnt/β-catenin signalling in p53R172H (PC) cells (Fig. 2C), which is supported by a general downregulation of Wnt pathway genes (SFig. 4A). Both, KrasG12D cells (KC; SFig. 4B) and p53R172H cells (PC; SFig. 4C) gene signatures positively correlated with Wnt5a-ROR signalling pathway.

To further investigate the activity of Wnt/β-catenin signalling we performed immunofluorescence for β-catenin in murine tissues fixed at 35 days p.i., using nuclear localisation as a surrogate marker of activity of the pathway. Nuclear β-catenin was undetectable in nuclei of both the control and KrasG12D (KC) cells (Fig. 4D, 4E; *p*=0.3035), indicating that Wnt/β-catenin signalling is not active in the non-eliminated KC cells, consistent with our transcriptional analysis. We found that levels of β-catenin significantly increased at RFP+: RFP- cell-cell contacts in KrasG12D (KC) tissues compared to controls (Fig. 4D, 4E; *p*=0.0347). To further investigate active Wnt signalling *in vivo*, we performed immunofluorescence for CD44 which is a target of β-catenin dependant and independent signalling (*47-49*). Consistent with previous reports (46), we observed CD44 at the cell membranes in PanINs (SFig. 4D). We found that CD44 was significantly increased at RFP+: RFP- cell-cell boundaries in KrasG12D (KC) tissues compared to RFP+: RFP- boundaries in wild type controls (Fig. 4G, 4H; KC versus control, *p*=0.0009). In contrast, CD44 was significantly reduced within a cluster of KrasG12D cells (KC; Fig. 4G, 4I; *p*=0.0455). We

asked whether increased CD44 at mutant-normal cell-cell boundaries was dependent on competitive normal-mutant interactions. We quantified CD44 at cell-cell contacts between RFP+/RFP- cells in KC tissues fixed following high dose tamoxifen induction (KC Megadose). We previously reported that KrasG12D cells are not eliminated from megadose tissues, where mutant cells occupy ~80% of the tissue (*4*). We found that CD44 levels were significantly lower at mutant-normal cell boundaries in megadose tissues compared to KrasG12D low dose tissues (KC versus KC Megadose; Fig 4G, 4H; p=0.0047), while CD44 levels were significantly higher between KrasG12D cells in megadose tissues (Fig. 4G, 4I; p=0.0341). Similarly, we found that CD44 was significantly increased at RFP+: RFP- cell-cell boundaries in p53R172H tissues (PC) compared to RFP+: RFP- boundaries in wild type controls (SFig. 4E; PC versus control, p=0.047). CD44 was significantly reduced within a cluster of p53R172H cells (SFig. 4F, PC versus control, p=0.0397). These data suggest that β-catenin-independent Wnt signalling is specifically increased in cells at mutant-normal boundaries of non-eliminated mutant cells *in vivo.*

Wnt signalling is required to prevent KrasG12D cell elimination *in vitro* and *in vivo*.

Next, we set out to test whether Wnt signalling was required to prevent cell elimination. We first repeated cell extrusion experiments using siScr-GFP-RasV12 or siMyc 1+2-GFP-RasV12 MDCK cells mixed with normal MDCK cells at 1:50 ratios, allowed cells to form cell-cell interactions and then treated with the porcupine inhibitor WNT-974 (or DMSO). Porcupine is an acyltransferase enzyme required for the lipidation and trafficking of Wnt proteins, which is a necessary step for ligand secretion (*50*). By inhibiting porcupine, Wnt ligands cannot be secreted and therefore cannot signal to cells. The proportion of non-extruded siMyc 1+2-GFP-RasV12 cells significantly reduced in the presence of WNT-974 (Fig. 5A, 5B; p<0.0005), compared to siScr-GFP-RasV12 treated cultures (Fig. 5A; p=0.6912). In cell confrontation assays, we found that WNT-974-treated siMyc 1+2-GFP-RasV12 cells efficiently retracted (SFig. 5A, 5B) and segregated from normal cells, compared to DMSO-treated siMyc 1+2-GFP-RasV12 controls. Quantification of the linearity of the boundary between colliding sheets of cells (*9*) confirmed this observation (SFig. 5C; WNT-974-treated cells: p=0.0020). Western blot analysis of total cell lysates isolated from siMyc 1+2-GFP-RasV12 cells treated with WNT-974 showed reduced p21 expression, while phospho-p38 expression increased, compared to DMSO treated siMyc 1+2-GFP-RasV12 cells (SFig. 5D, 5E).

Based on our RNA sequencing data showing an enrichment of Wnt5a signalling in KrasG12D cells (KC; Fig. 2B: Wnt5a-Ror signaling-M47822; Fig. 4B) and down-regulation of Wnt/β-catenin signalling at the transcriptional level (KC; Fig. 4C), we hypothesised that Wnt5a signalling may play a key role in protecting KrasG12D cells from being eliminated.

Moreover, Wnt5a activates cancer cell dormancy in metastatic niches (*43, 44*). In MDCK cells, overexpression of RasV12 induces expression and secretion of Wnt5a in a porcupine-dependent manner (*51*), suggesting porcupine inhibition in our experiments blocks endogenous Wnt secretion, including Wnt5a. We assessed the effect of Wnt5a treatment on normal-RasV12 cell-cell interactions by pre-treating GFP-RasV12 cells with recombinant Wnt5a (or PBS) before mixing with normal MDCK cells in 1:50 ratios (recombinant Wnt5a was maintained for the entire experiment). We found that the proportion of non-extruded GFP-RasV12 cells significantly increased in the presence of Wnt5a (Fig. 5C, left panels; 5D, solid bars, p=0.0109 and 5E, solid bars, p=0.005). Consistently, the effects of Wnt5a were reversed in the presence of a porcupine inhibitor (WNT-974; Fig. 5C, middle panel; 5D, hached bars; p=0.0114) and in the presence of the Frizzled (Fzd) receptor antagonist (*52*) OMP-18R5 (Fig. 5C, right panel; 5E, striped bars; p=0.0004) compared to DMSO-treated controls, resulting in a significant decrease in non-extruded GFP-RasV12 cells. Taken together, we conclude that active Wnt signalling (e.g., via Wnt5a) abrogates normal-mutant cell-cell interactions to allow RasV12 cells to be retained in an epithelium. Inhibition of Wnt signalling (via Wnt ligand secretion or Frizzled receptor binding) switches mutant cell retention to cell elimination.

Finally, we set out to functionally test whether active Wnt signalling is necessary for mutant cell retention *in vivo*. Using 6-8-week-old adult KrasG12D (KC) mice, we first induced low level recombination in tissues, waited for 35 days p.i. to allow for cell competition to proceed and for most mutant cells to be eliminated, and then administered the porcupine inhibitor WNT-974 (or DMSO in corn oil vehicle) for a period of 4 weeks (Fig. 5F). To validate Wnt inhibition in tissues *in vivo*, we quantified CD44 fluorescence at mutant-normal cell boundaries and within RFP+ clusters in KrasG12D (KC) pancreas tissues treated with WNT-974 or vehicle. We found that levels of CD44 fluorescence significantly decreased in WNT-974 treated tissues compared to vehicle (SFig. 5F, p=0.0467), suggesting Wnt activity is reduced following treatment with porcupine inhibitor. Using global RFP fluorescence per tissue area as a readout of mutant cell fate, we measured a significant decrease in RFP fluorescence in the WNT-974-treated cohort compared to vehicle-treated animals (Fig. 5G, 5H; p=0.0003). Strikingly, we found that porcupine inhibition also induced a significant decrease in RFP fluorescence in p53R172H (PC) tissues compared to vehicle treated controls (SFig. 5G, 5H; p=<0.0001). Taken together, our data show that inhibition of Wnt pathway induces the elimination of mutant KrasG12D or p53R172H cells from pancreas tissues *in vivo*; however, Wnt inhibition is not sufficient to remove all mutant cells from tissues, suggesting Wnt-independent mechanisms are also required. Nonetheless, our data support a model whereby activation of Wnt signalling allows mutant cells to avoid cell elimination and survive in the pancreas.

Discussion

Tissue homeostasis is fundamental to healthy aging of an organism and cell competition is an important regulator of tissue health. Here, we extend our previously published results (*4*) to show that like KrasG12D-expressing cells, genetically mutant p53R172H-expressing cells compete with normal cells for survival in the adult pancreas and are often eliminated. We report that cell elimination is inefficient, and a proportion of KrasG12D- or p53R172H-expressing cells are never eliminated from the tissue, suggesting these cells have a survival advantage. We identified active Wnt signalling as a general mechanism required to protect KrasG12D or p53R172H cells from cell elimination *in vivo*. We also reveal cell cycle arrest/cell dormancy as a second mechanism whereby KrasG12D cells avoid cell elimination (SFig. 5I). Interestingly, co-expression of p53R172H and KrasG12D in the same cell, provides all mutant cells with a survival advantage and 'double mutant' KPC cells are never eliminated. In MDCK cells, ectopic expression of p53R175H/p53R273H mutations in few cells surrounded by normal cells triggers necroptosis and elimination of the p53 mutant cells (*40*); however, expression of p53R273H mutations in RasV12 monolayers prevents p53 mutant cell death (*40*), supporting our observations, and suggesting 'double mutant' KPC cells may also override cell death signals *in vivo*. Indeed, our RNA sequencing data suggest cells expressing p53 mutations downregulate the apoptosis pathway (Fig. 2B, SFig. 2E). Future work will determine whether retention of mutant cells is stochastic or is controlled by cell intrinsic/extrinsic properties of mutant cells and the local tissue niche.

TP53 is an important regulator of cell competition. In MDCK cells (*53, 54*) and in developing embryos (*55, 56*), mutant-normal cell competition triggers an elevation in p53 levels and p53 activity in prospective 'losers' and this is required for mutant cell elimination (*55*). It is generally perceived that mutant p53 proteins (such as p53R172H) act in a dominant negative manner in cells by reducing wild type p53 activity (*57*). Studies in the adult hematopoietic system (*58, 59*) and oesophagus (*13, 60*) illustrate that competition outcomes are dependent on relative rather than absolute levels of p53 and are apparent only when cells are under mild stress. Whether cell competition outcomes we describe here are triggered by differentials in p53 activity between mutant and wild type neighbours requires further investigation.

Here, we show that Ras mutant cells are not eliminated when in a cell cycle arrested state. KrasG12D cells that are not eliminated from the pancreas upregulate cell dormancy signatures and pathways known to induce cell dormancy (e.g., Unfolded protein response, Wnt5a-ROR signalling, Hypoxia) (*61*), suggesting cell dormancy protects KrasG12D cells from cell elimination *in vivo*. Cell stress responses are major triggers of cell dormancy (*62*). It is possible that non-eliminated KrasG12D cells enter a dormant state in response to competition-induced stress, overriding cell elimination and surviving in tissues. Studies in

Drosophila melanogaster models demonstrate that cell competition outcomes are a consequence of cellular stress responses activated in 'loser' cells (*63-68*). Taking these studies into consideration, our transcriptomic data infer that non-eliminated KrasG12D cells upregulate gene signatures reminiscent of 'loser' phenotypes (e.g., Glycolysis (*7*), Unfolded protein response (*69*), p53 (*12, 40, 54-56, 70*), oxidative stress (*71*), NRF2 pathway (*64, 71, 72*). Thus, cell dormancy may act to restrict expansion of 'unfit' KrasG12D cells in the absence of an efficient tissue clearance mechanism and without drastically reducing cell numbers. This would be particularly relevant to adult pancreas, which has limited proliferative capacity (*73*). Indeed, we never observe compensatory proliferation in neighbours following mutant cell clearance (*4*) (SFig. 3A). Future studies are required to determine whether normal-mutant interactions in the adult pancreas induce cellular stress responses in genetically mutant cells and whether this in turn activates cell dormancy.

We demonstrate that Wnt signalling is critical for mutant cells to avoid cell elimination and remain in the pancreatic epithelium. Wnt is a key regulator of cell competition, and cells with high Wnt activity are generally 'winner' cells (*16-18, 74*). Cell competition triggered by differentials in Wnt activity also maintains a Wnt morphogen gradient in development (*75*). Cells high or low in Wnt activity (relative to neighbours) causes an imbalance in E-cadherin/β-catenin levels at cell-cell junctions, which in turn triggers a stress response and apoptosis of 'loser' cells (*75*). We previously showed that prior to KrasG12D cell elimination, E-cadherin decreased specifically at normal-mutant cell-cell junctions in pancreas tissues *in vivo.* Moreover, increased E-cadherin at normal-mutant boundaries prevented KrasG12D cell elimination (*4*). Here, we show that Wnt signalling is active at cell-cell junctions between normal and mutant cells *in vivo*. Gene expression data indicate Wnt/β-catenin signalling is inactive and instead, non-canonical Wnt5a-Ror signalling is active in non-eliminated KrasG12D cells. We also show that apical extrusion and cell segregation of RasV12 cells from normal cells are inhibited in the presence of Wnt5a. Interestingly, Wnt5a has been shown to induce and maintain cancer cell dormancy in metastatic niches by negatively regulating canonical Wnt/β-catenin signalling (*43, 44*). An exciting future direction of this work will be to elucidate whether the cell dormancy phenotype we describe here is regulated via Wnt-dependent mechanisms described for dormant metastatic cancer cells. Transcriptional profiling of non-eliminated KrasG12D cells support a mechanism whereby Wnt signalling at KrasG12D-normal cell-cell boundaries is not driving a stem or cycling cell state. We also show that inhibition of Wnt restores cell extrusion and cell segregation of cell cycle arrested RasV12 cells from normal cells *in vitro*, suggesting a mechanistic link between active Wnt and cell dormancy *in vivo* is plausible (SFig. 5I).

KRAS and *TP53* mutations are key drivers of pancreatic ductal adenocarcinoma. Single cell profiling of pancreatic tumorigenesis in mouse models demonstrates that *Kras*

mutant cells are very heterogeneous and show signatures of tumorigenesis even before pre-malignant lesions are established (*76*). Our RNA sequencing data confirm this early transformation and cellular heterogeneity profile of KrasG12D cells. Pancreatic cancer is a devastating disease, which is generally diagnosed at late and incurable stages. An improved understanding of the biology of how pancreatic cancer starts and grows in adult tissues will inform the development of new early detection methods. Our results challenge the current understanding of how cancers start in the adult pancreas and suggest that genetically mutant cells must override tissue homoeostasis mechanisms to survive in tissues, prior to transformation/expansion.

Author Contributions

Conceptualization, CH; Data curation, BS-B; Experimental design, BS-B, CH; Funding acquisition, CH; Investigation & Analysis: BS-B, CH, JPM, OJS; Methodology, BS-B, MA; Validation, BS-B; Writing original draft, BS-B, CH; Writing review & editing, BS-B, CH; Resources, JPM, OJS; Supervision, CH.

Acknowledgements

We thank Angela Marchbank and colleagues at School of Biosciences Genome Hub (Cardiff University) for technical support with RNA sequencing experiments. We thank Toby Phesse and Valerie Meniel (European Cancer Stem Cell Research Institute, School of Biosciences, Cardiff University) for Wnt antagonists, PCR primers and helpful discussions on the Wnt pathway. We thank F. Afonso (European Cancer Stem Cell Research Institute, School of Biosciences, Cardiff University) for critical reading of the manuscript and helpful discussions. B.S. and M.A. were supported by Cancer Research UK (CRUK) Early Detection project grant (A27838) to C.H. O.J.S. and J.P.M. were supported by Cancer Research UK core funding to the CRUK Scotland Institute (A17196 and A31287) to O.J.S. laboratory (A21139) and to J.P.M. laboratory (A29996). B.S-B. is currently funded by a Pancreatic Cancer UK Career Foundation Fellowship (CFF2022_05). This study was supported by Cancer Research UK (CRUK) Early Detection project grant (A27838) to C.H. The manuscript was critically reviewed by Catherine Winchester (CRUK Scotland Institute).

Methods

Mouse lines, Induction of Cre recombinase *in vivo*, Inhibition of Wnt *in vivo*.

Pdx1-Cre^{ERT}(*77*), *LSL-Kras*$^{G12D/+}$(*78*), LSL-*Trp53*$^{R172H/+}$ (*79*), *Rosa26*$^{LSL\text{-}tdRFP}$ (*80*) mouse lines have all been previously described. Animals were housed in conventional pathogen-free animal facilities and experiments were conducted in accordance with UK Home Office regulations (ASPA 1986 & EU Directive 2010) under the guidelines of Cardiff University Animal Welfare and Ethics Committee. Mice were genotyped by PCR analysis following standard methods and using primer sequences in (*4*). Both male and female 6-8-week-old experimental and control mice were injected with intraperitoneal injection of tamoxifen in corn oil as previously described (*4*). Low recombination levels were obtained with a tamoxifen dose of 1µg/40g bodyweight once, while high recombination (megadose) was induced by three injections of 9mg/40g over 5 days (*4*). Pancreata were harvested at 7-, 35-, 70- or 140-days post tamoxifen induction. To test the functional role of Wnt signalling *in vivo*, 6-8-week-old experimental and control mice were induced with low dose tamoxifen, aged to 35-days post induction of Cre recombinase (p.i.) and treated with WNT-974 1.5mg/kg or vehicle (DMSO) in corn oil by oral gavage, five days per week for four weeks. At the end of the treatment pancreatic tissue was harvested and treated as described below. No statistical method was used to pre-determine sample size. For most animal studies, experiments were not randomized, and investigators were not blinded to allocation during experiments. To test the functional role of Wnt signalling mice were randomly allocated into vehicle or WNT-974 treated groups. All experiments were reproduced using at least three animals of each genotype.

Tissue staining.

For histological observation, pancreas was harvested at specified timepoints and fixed in 10% neutral buffered formalin overnight at 4ºC. Then pancreas was dissected into two pieces (head-body/body-tail) and embedded either in paraffin or OCT matrix. FFPE embedded pancreas was sectioned (7µm thickness) and stained with specific antibodies (table 1). Anti-RFP, anti-cleaved caspase-3, and anti-Ki-67 staining were performed via immunohistochemistry (IHC) in FFPE tissue sections. Tissues sections were dewaxed and rehydrated. For antigen retrieval, tissue sections were incubated for 15 minutes at 37ºC in 20ug/ml Proteinase K diluted in TBS-T or boiled in citrate buffer pH 6 for 15 minutes (specified in table 1). Tissues were then blocked with 3% H_2O_2 for 20 or 10 minutes at room temperature (depending on the antigen retrieval method) respectively and 5% NGS TBS-T for 30-60 minutes at room temperature. Sections were then incubated overnight at 4ºC with the primary antibody diluted in 5% NGS TBS-T (see dilutions in table 1). Tissues were stained with the secondary antibody ImmPRESS goat anti-Rabbit (MP-7451, Vector Labs)

for 60 minutes at room temperature, followed by DAB chromogen (Peroxydase substrate kit, Vector Labs). Sections were dehydrated and mounted with DPX (Sigma-Aldrich) and scanned using the Axio Scan Z1 slide scanner (Zeiss) 20X magnification. Immunofluorescence (IF) co-staining using either anti-CD44 and anti-RFP (Rockland) was performed in FFPE tissues slices using the same antigen retrieval and primary antibody incubations as described for IHC, followed by Alexa fluor secondary antibody incubation for 60 minutes at room temperature and Hoechst (ThermoFisher) (table 1) and mounted using Mowiol (Sigma-Aldrich).

For β-catenin and RFP (Creative Diagnostics) IF staining, pancreas was embedded in butyl-methyl methacrylate plastic (BMMA) under UV following dehydration and resin infiltration (*4*). Tissue was sectioned in 2µm thick slices and rehydrated. Tissue staining followed the same protocol as IF in FFPE sections. Antigen retrieval and antibody concentrations are listed in table 1.

Global levels of endogenous RFP were measured in 10µm formalin fixed OCT frozen sections, as previously described (*4*). RFP positive area was averaged from 3 tissue slices per mouse separated by at least 20µm between each section. Fluorescence imaging was carried out on a Zeiss LSM710 confocal microscope.

To assess the presence of PanIN lesions, FFPE sections were stained with Alcian blue as previously described (*4*). β-galactosidase activity was determined using the Cell Signaling Senescence β-galactosidase Staining kit (9860) using the manufacturers' instructions.

Image analysis.

The percentage of RFP+ tissue area was determined using endogenous RFP levels quantified as described in (*4*). Using Fiji (RRID:SCR_002285) software,(*81*) positive areas were thresholded using RFP fluorescence. Tissue autofluorescence was used to determine total tissue area. The percentage of RFP+ ducts were analysed using E-cadherin/RFP/Hoechst-stained sections to identify ducts. At least 20 ducts were quantified per mouse and ducts were considered positive when they contained at least one RFP+ cell. The percentage of RFP+ cells in pancreatic islets were scored in FFPE IHC sections stained with anti-RFP antibody and using 'positive cell count' tool in QuPath-0.4.1 software. RFP positive cluster size, perimeter and area were determined in FFPE IHC sections stained with anti-RFP antibody and using QuPath-0.4.1 software by analysing shape features of RFP positive (DAB positive) areas. Ki-67 positive and Cleaved Caspase-3 positive cells were analysed using QuPath-0.4.1 positive cell count feature.

CD44 and β-catenin in clusters fluorescence intensities were quantified masking RFP positive cells/clusters (AF568) and quantifying mean fluorescence intensity in AF488 (CD44 and β-catenin) in Fiji. CD44 and β-catenin fluorescence intensity at the border between RFP positive and negative cells were quantified by measuring mean fluorescence intensity of 2.43x2.43-pixel circles (ROIs) along the membrane (RFP+/RFP-) separated by approximately 5 pixels. CD44 fluorescence in clusters was quantified by masking RFP+ (AF568) areas and quantifying mean fluorescence intensity for CD44 (AF488). β-catenin fluorescence in nuclei was quantified by masking nuclei (Hoechst) and quantifying mean fluorescence intensity for β-catenin (AF488) in RFP+ cells. To avoid noise associated with tissue autofluorescence, fluorescence intensity measurements were made relative to image global mean fluorescence intensity (AF488).

Pancreas digestion and RNA Sequencing

Pancreas tissues were harvested 35 days post low-dose tamoxifen induction. To reach the minimum of 5000 cells and a minimum of 100ng RNA/sample for bulk RNA sequencing, we combined three pancreas tissues of the same genotype to produce one sample per genotype. Each sample was replicated three times to generate three biological repeats per genotype for sequencing. Pancreas tissues were digested as previously described (*82*). Using an EGTA-based buffer the pancreas from each mouse was inflated and slightly digested with collagenase. The tissue was chopped and further digested using a calcium-based buffer with collagenase. Single cell digested tissue was stained with lectin PNA-A488 (ThermoFisher) and DAPI (ThermoFisher Scientific). DAPI negative, lectin positive, RFP positive cells were sorted using the FACS Aria Fusion sorter. A minimum of 5,000 cells were sorted for each sample. RNA was extracted using the RNeasy Micro kit (Qiagen) following the manufacturer's recommendations. Paired-end sequencing was performed using Sanger sequencing Illumina 1.9. Sequenced reads Fastq files were quality-checked using FastQC. Reads were aligned to the mouse genome (Ensembl-GRCm38 *Mus musculus*) using the STAR package, and reads were counted using the FeatureCounts package, after removing duplicates using MarkDuplicates from GATK. Differential expression was normalised and calculated using Deseq2, comparing the different genotypes against the Control. Finally, GSEA 4.2.2 software was used for enrichment analysis of different pathways and GraphPad Prism 10.0.2 for Heatmap graphs and normalised enrichment score (NES) graphs. The RNAseq data generated during this study are available at NCBI GEO.

MDCK cell lines and *In vitro* experiments.

For cell extrusion experiments, MDCK-pTR GFP–RasV12 cells were first treated with tetracycline (2µg/mL) to induce GFP-RasV12 expression (*5, 9*). RasV12 cells were either treated with siRNA oligos or with recombinant Wnt5a (see below), then trypsinized (Merck) and combined with parental MDCK cells at a ratio of 1:50. Cells were plated at a density of 2.5 x 10^5 cells per well in MW24 plates (Corning) carrying 18mm diameter glass cover slips (VWR). Mixed cells were incubated for 48h at 37ºC before fixed with 4% Formaldehyde (ThermoFisher Scientific). Cells were then permeabilized and stained with phalloidin and Hoechst (table 1) and imaged using a Zeiss confocal LSM 710. GFP-RasV12 cells were considered non-extruded when more than 30% of their cytoplasm was basally protruded. Three technical replicates per experiment in three experiments (i.e., using three independent frozen stocks of parental and GFP-RasV12 MDCK cells) were performed and at least 150 GFP-RasV12 cells were quantified per replicate. To assess proliferation, cells were fixed 48h after siMyc1+2 transfection, permeabilized with 0.05% SDS (Sigma-Aldrich) and 0.05% Triton X100 (Sigma-Aldrich) solution and stained with anti-Ki-67 primary antibody, and goat anti-Rabbit AF568 secondary antibody and Hoechst (ThermoFisher Scientific) (table 1). At least 30 extruded and 30 non-extruded cells were quantified in siMyc 1+2 treated cells per experimental replicate. We performed three technical replicates per experiment in three experiments.

For c-Myc silencing, tetracycline induced GFP-RasV12 cells were transfected with 100ng siRNA oligos targeting *Myc* using Lipofectamine 3000 (Invitrogen) (siRNA siMyc1: AAGACGUUGUGUGUUCGCCUC – as GAGGCGAACACACAACGUCUU, siRNA siMyc2: AAUUUCAACUGUUCUCGCCGC – as GCGGCGAGAACAGUUGAAAUU and siScr)[24]. For cell extrusion experiments, cells were trypsinized and mixed with parental MDCK cells 24h after transfection.

For Wnt5a experiments tetracycline induced GFP-RasV12 cells were treated with 100ng/mL recombinant human/mouse Wnt5a (R&D Systems) or PBS (control-Sigma-Aldrich) for 24h and then mixed with parental MDCK cells. Wnt5a treatment was maintained during the whole experiment. WNT-974 (Stratech) porcupine inhibitor (1µM) or OMP-18R5 (10mg/mL) was added to the medium 8h after GFP-RasV12 and MDCK cells were mixed and plated. DMSO treated GFP-RasV12 cells were used as control for both inhibitors.

Confrontation assays were carried out as described (*9*). 1x10^4 cells were plated in inserts (Ibidi) in MW24 plates (Corning), allowed to form monolayers (8h) before removing the insert and moving the plate to IncuCyte S3 (Sartorius) for live cell imaging. Images were captured every 15min for 48h. siMyc/siScr-GFP-RasV12 cells were plated 24h after transfection and

inserts were removed 8h post transfection. WNT-974 porcupine inhibitor (Stratech)/DMSO (Sigma-Aldrich) was added to the medium when inserts were removed. Retraction was measured as the distance GFP-RasV12 cells migrated during 24h, following initial cell-cell collision with MDCK cells. Coefficient of boundary smoothness was measured using Fiji in cell confrontation assays at the end of the 24 h experiment and as previously described (*9*). We performed three technical replicates per experiment in three experiments.

Western blotting was performed using GFP-RasV12 cell lysates transfected with siMyc/siScr siRNAs at 48h post transfection (SFig. 3E), treated for 48h with WNT-974/DMSO 24h post-transfection (SFig. 5D). Cells were lysed using laemmli buffer (0.0625 M Tris base, 2% SDS, 10% glycerol). Proteins were separated on 12% polyacrylamide gels under reducing PAGE conditions. Proteins were then transferred to PVDF membranes (Immobilon-P, Merck) using wet transfer (1h 100V). Membranes were blocked in 5% milk TBS-T for 1h and antibodies were added in the same buffer at the concentrations listed in table 1 for overnight at 4ºC or 2h at room temperature. Secondary antibodies (table 1) were added in 5% milk TBS-T and membranes were developed using ECL luminol kit (Merck) and chemiluminescence films (Amersham Hyperfilm ECL, GE Healthcare). Protein levels were quantified using Fiji (RRID:SCR_002285) software 'Gels' tool.

Real time cell confluency was measured using Incucyte S3 live cell imaging instrument and software (v2020). $1x10^3$ cells siMyc/siScr-GFP-RasV12 cells were plated 24h after transfection with siMyc/siScr siRNAs in MW96 (Corning). Images were captured every 15min for 48h. We performed three technical replicates per experiment in three experiments.

Statistical tests

Statistical analyses were performed using GraphPad Prism 10 software. Normally distributed data, as determined by the Shapiro-Wilke test or D'Agostino and Pearson test were analysed using unpaired Student's t tests. A p value of <0.05 was taken as significant and a rejection of the null hypothesis. No statistical method was used to pre-determine sample size. Definition of n is in the figure legends. Gene set enrichment analysis (GSEA) was performed using GSEA 4.2.2 software. GSEA was used to identify gene sets that were differentially expressed between two groups of samples. Gene sets were considered enriched if they had a false discovery rate (FDR) of less than 0.25. Heatmaps were created by computing normalised gene counts for each individual sample into row z-scores.

Table 1

Antibody and fluorescence stains	Application	Antigen Retrieval	Dilution	Source	Identifier
Ki-67	IHC, IF	ProK 15’	1:500	Abcam	ab16667
CC-3	IHC	Citrate pH6 15’	1:300	Cell Signaling	9661s
RFP	IHC, IF	ProK 15’	1:500	Rockland	600-401-379
Lectin PNA-A488	FACS			Invitrogen	L21409
c-Myc	WB		1:500	Santa Cruz	sc788
Phospho-p38	WB		1:1000	Cell Signaling	9211s
p38a	WB		1:1000	Santa Cruz	sc136210
Vinculin	WB		1:1000	Sigma Aldrich	V4505
Phosphor-ERK	WB		1:1000		
ERK	WB		1:1000	Cell Signaling	
p21WAP/Cip	WB		1:1000	Sigma Aldrich	P1484
CD44	IF	ProK 15’	1:25	Cell Signaling	3570S
β-catenin	IF	Citrate pH6 15’	1:50	BD Biosciences	610154
RFP	IF	Citrate pH6 15’	1:500	Creative Diagnosis	DPATB-H83194
E-cadherin	IF	Citrate pH6 15’	1:1000	BD Biosciences	610182
goat anti-rabbit AF568	IF		1:1000	ThermoFisher	A-11011
donkey anti-mouse AF488			1:1000	ThermoFisher	A-21202
goat anti-rabbit AF488	IF		1:1000	ThermoFisher	A-11008
goat anti-rabbit HRP	WB		1:5000	Vector Laboratories	MP-7451-15
goat anti-mouse HRP	WB		1:5000	Vector Laboratories	MP-7802-15
Phalloidin	IF		1:1000	Sigma Aldrich	65906
Hoechst			1:1000	ThermoFisher Scientific	H3570

References

1. C. Bielmeier *et al.*, Interface Contractility between Differently Fated Cells Drives Cell Elimination and Cyst Formation. *Curr Biol* **26**, 563-574 (2016).

2. O. Klipa, F. Hamaratoglu, Cell elimination strategies upon identity switch via modulation of apterous in Drosophila wing disc. *PLoS Genet* **15**, e1008573 (2019).

3. S. Brown *et al.*, Correction of aberrant growth preserves tissue homeostasis. *Nature* **548**, 334-337 (2017).

4. W. Hill *et al.*, EPHA2-dependent outcompetition of KRASG12D mutant cells by wild-type neighbors in the adult pancreas. *Curr Biol* **31**, 2550-2560 e2555 (2021).

5. C. Hogan *et al.*, Characterization of the interface between normal and transformed epithelial cells. *Nat Cell Biol* **11**, 460-467 (2009).

6. M. Kajita *et al.*, Interaction with surrounding normal epithelial cells influences signalling pathways and behaviour of Src-transformed cells. *J Cell Sci* **123**, 171-180 (2010).

7. S. Kon *et al.*, Cell competition with normal epithelial cells promotes apical extrusion of transformed cells through metabolic changes. *Nat Cell Biol* **19**, 530-541 (2017).

8. M. Norman *et al.*, Loss of Scribble causes cell competition in mammalian cells. *J Cell Sci* **125**, 59-66 (2012).

9. S. Porazinski *et al.*, EphA2 Drives the Segregation of Ras-Transformed Epithelial Cells from Normal Neighbors. *Curr Biol* **26**, 3220-3229 (2016).

10. S. M. van Neerven, L. Vermeulen, Cell competition in development, homeostasis and cancer. *Nat Rev Mol Cell Biol* **24**, 221-236 (2023).

11. N. E. Baker, Emerging mechanisms of cell competition. *Nat Rev Genet* **21**, 683-697 (2020).

12. D. Fernandez-Antoran *et al.*, Outcompeting p53-Mutant Cells in the Normal Esophagus by Redox Manipulation. *Cell Stem Cell* **25**, 329-341 e326 (2019).

13. K. Murai *et al.*, Epidermal Tissue Adapts to Restrain Progenitors Carrying Clonal p53 Mutations. *Cell Stem Cell* **23**, 687-699 e688 (2018).

14. A. Sasaki *et al.*, Obesity Suppresses Cell-Competition-Mediated Apical Elimination of RasV12-Transformed Cells from Epithelial Tissues. *Cell Rep* **23**, 974-982 (2018).

15. M. P. Alcolea *et al.*, Differentiation imbalance in single oesophageal progenitor cells causes clonal immortalization and field change. *Nat Cell Biol* **16**, 615-622 (2014).

16. D. J. Flanagan *et al.*, NOTUM from Apc-mutant cells biases clonal competition to initiate cancer. *Nature* **594**, 430-435 (2021).

17. S. M. van Neerven *et al.*, Apc-mutant cells act as supercompetitors in intestinal tumour initiation. *Nature* **594**, 436-441 (2021).

18. M. K. Yum *et al.*, Tracing oncogene-driven remodelling of the intestinal stem cell niche. *Nature* **594**, 442-447 (2021).

19. W. Hill, C. Hogan, Normal epithelial cells trigger EphA2-dependent RasV12 cell repulsion at the single cell level. *Small GTPases* **10**, 305-310 (2019).

20. S. Lanfredini, A. Thapa, E. O'Neill, RAS in pancreatic cancer. *Biochem Soc Trans* **47**, 961-972 (2019).

21. M. A. Collins *et al.*, Oncogenic Kras is required for both the initiation and maintenance of pancreatic cancer in mice. *J Clin Invest* **122**, 639-653 (2012).

22. P. Bailey *et al.*, Genomic analyses identify molecular subtypes of pancreatic cancer. *Nature* **531**, 47-52 (2016).

23. J. P. Morton *et al.*, Mutant p53 drives metastasis and overcomes growth arrest/senescence in pancreatic cancer. *Proc Natl Acad Sci U S A* **107**, 246-251 (2010).

24. T. E. Woolley, W. Hill, C. Hogan, Accounting for dimensional differences in stochastic domain invasion with applications to precancerous cell removal. *J Theor Biol* **541**, 111024 (2022).

25. S. R. Hingorani *et al.*, Preinvasive and invasive ductal pancreatic cancer and its early detection in the mouse. *Cancer Cell* **4**, 437-450 (2003).

26. B. M. Flowers *et al.*, Cell of Origin Influences Pancreatic Cancer Subtype. *Cancer Discov* **11**, 660-677 (2021).

27. Z. Ma *et al.*, Single-Cell Transcriptomics Reveals a Conserved Metaplasia Program in Pancreatic Injury. *Gastroenterology* **162**, 604-620 e620 (2022).

28. K. Nozaki *et al.*, A molecular signature of gastric metaplasia arising in response to acute parietal cell loss. *Gastroenterology* **134**, 511-522 (2008).

29. J. Benn, R. J. Schneider, Hepatitis B virus HBx protein deregulates cell cycle checkpoint controls. *Proc Natl Acad Sci U S A* **92**, 11215-11219 (1995).

30. T. Kasai, Y. Iwanaga, H. Iha, K. T. Jeang, Prevalent loss of mitotic spindle checkpoint in adult T-cell leukemia confers resistance to microtubule inhibitors. *J Biol Chem* **277**, 5187-5193 (2002).

31. V. A. van der Weijden, A. Bulut-Karslioglu, Molecular Regulation of Paused Pluripotency in Early Mammalian Embryos and Stem Cells. *Front Cell Dev Biol* **9**, 708318 (2021).

32. J. E. Davis, Jr., J. Kirk, Y. Ji, D. G. Tang, Tumor Dormancy and Slow-Cycling Cancer Cells. *Adv Exp Med Biol* **1164**, 199-206 (2019).

33. E. Dhimolea *et al.*, An Embryonic Diapause-like Adaptation with Suppressed Myc Activity Enables Tumor Treatment Persistence. *Cancer Cell* **39**, 240-256 e211 (2021).

34. A. M. Hussein, N. Balachandar, J. Mathieu, H. Ruohola-Baker, Molecular Regulators of Embryonic Diapause and Cancer Diapause-like State. *Cells* **11**, (2022).

35. R. S. Kim *et al.*, Dormancy signatures and metastasis in estrogen receptor positive and negative breast cancer. *PLoS One* **7**, e35569 (2012).

36. D. B. Fox *et al.*, NRF2 activation promotes the recurrence of dormant tumour cells through regulation of redox and nucleotide metabolism. *Nat Metab* **2**, 318-334 (2020).

37. S. Easwaran, M. Van Ligten, M. Kui, D. J. Montell, Enhanced germline stem cell longevity in Drosophila diapause. *Nat Commun* **13**, 711 (2022).

38. K. Itahana *et al.*, A role for p53 in maintaining and establishing the quiescence growth arrest in human cells. *J Biol Chem* **277**, 18206-18214 (2002).

39. A. J. Wiecek *et al.*, Genomic hallmarks and therapeutic implications of G0 cell cycle arrest in cancer. *Genome Biol* **24**, 128 (2023).

40. H. Watanabe *et al.*, Mutant p53-Expressing Cells Undergo Necroptosis via Cell Competition with the Neighboring Normal Epithelial Cells. *Cell Rep* **23**, 3721-3729 (2018).

41. D. Dominguez-Sola, J. Gautier, MYC and the control of DNA replication. *Cold Spring Harb Perspect Med* **4**, (2014).

42. R. Scognamiglio *et al.*, Myc Depletion Induces a Pluripotent Dormant State Mimicking Diapause. *Cell* **164**, 668-680 (2016).

43. M. E. Fane *et al.*, Stromal changes in the aged lung induce an emergence from melanoma dormancy. *Nature* **606**, 396-405 (2022).

44. D. Ren *et al.*, Wnt5a induces and maintains prostate cancer cells dormancy in bone. *J Exp Med* **216**, 428-449 (2019).

45. J. B. Cordero, O. J. Sansom, Wnt signalling and its role in stem cell-driven intestinal regeneration and hyperplasia. *Acta Physiol (Oxf)* **204**, 137-143 (2012).

46. D. J. Flanagan *et al.*, Frizzled7 functions as a Wnt receptor in intestinal epithelial Lgr5(+) stem cells. *Stem Cell Reports* **4**, 759-767 (2015).

47. A. Abedini, C. Sayed, L. E. Carter, D. Boerboom, B. C. Vanderhyden, Non-canonical WNT5a regulates Epithelial-to-Mesenchymal Transition in the mouse ovarian surface epithelium. *Sci Rep* **10**, 9695 (2020).

48. S. K. Dissanayake *et al.*, The Wnt5A/protein kinase C pathway mediates motility in melanoma cells via the inhibition of metastasis suppressors and initiation of an epithelial to mesenchymal transition. *J Biol Chem* **282**, 17259-17271 (2007).

49. V. J. Wielenga *et al.*, Expression of CD44 in Apc and Tcf mutant mice implies regulation by the WNT pathway. *Am J Pathol* **154**, 515-523 (1999).

50. D. J. Flanagan, S. A. Woodcock, C. Phillips, C. Eagle, O. J. Sansom, Targeting ligand-dependent wnt pathway dysregulation in gastrointestinal cancers through porcupine inhibition. *Pharmacol Ther* **238**, 108179 (2022).

51. H. K. Lin *et al.*, Caveolin-1 down-regulation is required for Wnt5a-Frizzled 2 signalling in Ha-Ras(V12) -induced cell transformation. *J Cell Mol Med* **22**, 2631-2643 (2018).

52. D. J. Flanagan *et al.*, Frizzled-7 Is Required for Wnt Signaling in Gastric Tumors with and Without Apc Mutations. *Cancer Res* **79**, 970-981 (2019).

53. K. Kozyrska *et al.*, p53 directs leader cell behavior, migration, and clearance during epithelial repair. *Science* **375**, eabl8876 (2022).

54. L. Wagstaff *et al.*, Mechanical cell competition kills cells via induction of lethal p53 levels. *Nat Commun* **7**, 11373 (2016).

55. G. Zhang *et al.*, p53 pathway is involved in cell competition during mouse embryogenesis. *Proc Natl Acad Sci U S A* **114**, 498-503 (2017).

56. S. Bowling *et al.*, Author Correction: P53 and mTOR signalling determine fitness selection through cell competition during early mouse embryonic development. *Nat Commun* **9**, 3123 (2018).

57. S. Pilley, T. A. Rodriguez, K. H. Vousden, Mutant p53 in cell-cell interactions. *Genes Dev* **35**, 433-448 (2021).

58. T. Bondar, R. Medzhitov, p53-mediated hematopoietic stem and progenitor cell competition. *Cell Stem Cell* **6**, 309-322 (2010).

59. A. Marusyk, C. C. Porter, V. Zaberezhnyy, J. DeGregori, Irradiation selects for p53-deficient hematopoietic progenitors. *PLoS Biol* **8**, e1000324 (2010).

60. K. Murai *et al.*, p53 mutation in normal esophagus promotes multiple stages of carcinogenesis but is constrained by clonal competition. *Nat Commun* **13**, 6206 (2022).

61. E. Risson, A. R. Nobre, V. Maguer-Satta, J. A. Aguirre-Ghiso, The current paradigm and challenges ahead for the dormancy of disseminated tumor cells. *Nat Cancer* **1**, 672-680 (2020).

62. M. S. Sosa, P. Bragado, J. Debnath, J. A. Aguirre-Ghiso, Regulation of tumor cell dormancy by tissue microenvironments and autophagy. *Adv Exp Med Biol* **734**, 73-89 (2013).

63. L. Baillon, F. Germani, C. Rockel, J. Hilchenbach, K. Basler, Xrp1 is a transcription factor required for cell competition-driven elimination of loser cells. *Sci Rep* **8**, 17712 (2018).

64. P. F. Langton, M. E. Baumgartner, R. Logeay, E. Piddini, Xrp1 and Irbp18 trigger a feed-forward loop of proteotoxic stress to induce the loser status. *PLoS Genet* **17**, e1009946 (2021).

65. B. Brown, S. Mitra, F. D. Roach, D. Vasudevan, H. D. Ryoo, The transcription factor Xrp1 is required for PERK-mediated antioxidant gene induction in Drosophila. *Elife* **10**, (2021).

66. N. Ochi *et al.*, Cell competition is driven by Xrp1-mediated phosphorylation of eukaryotic initiation factor 2alpha. *PLoS Genet* **17**, e1009958 (2021).

67. N. E. Baker, C. Montagna, Reducing the aneuploid cell burden - cell competition and the ribosome connection. *Dis Model Mech* **15**, (2022).

68. M. Kiparaki *et al.*, The transcription factor Xrp1 orchestrates both reduced translation and cell competition upon defective ribosome assembly or function. *Elife* **11**, (2022).

69. J. Zheng *et al.*, Differential Ire1 determines loser cell fate in tumor-suppressive cell competition. *Cell Rep* **42**, 113303 (2023).

70. A. M. Klein, D. E. Brash, P. H. Jones, B. D. Simons, Stochastic fate of p53-mutant epidermal progenitor cells is tilted toward proliferation by UV B during preneoplasia. *Proc Natl Acad Sci U S A* **107**, 270-275 (2010).

71. I. Kucinski, M. Dinan, G. Kolahgar, E. Piddini, Chronic activation of JNK JAK/STAT and oxidative stress signalling causes the loser cell status. *Nat Commun* **8**, 136 (2017).

72. W. Hirose *et al.*, Selective Elimination of NRF2-Activated Cells by Competition With Neighboring Cells in the Esophageal Epithelium. *Cell Mol Gastroenterol Hepatol* **15**, 153-178 (2023).

73. J. Burclaff, J. C. Mills, Plasticity of differentiated cells in wound repair and tumorigenesis, part I: stomach and pancreas. *Dis Model Mech* **11**, (2018).

74. J. P. Vincent, G. Kolahgar, M. Gagliardi, E. Piddini, Steep differences in wingless signaling trigger Myc-independent competitive cell interactions. *Dev Cell* **21**, 366-374 (2011).

75. Y. Akieda *et al.*, Cell competition corrects noisy Wnt morphogen gradients to achieve robust patterning in the zebrafish embryo. *Nat Commun* **10**, 4710 (2019).

76. C. Burdziak *et al.*, Epigenetic plasticity cooperates with cell-cell interactions to direct pancreatic tumorigenesis. *Science* **380**, eadd5327 (2023).

77. G. Gu, J. Dubauskaite, D. A. Melton, Direct evidence for the pancreatic lineage: NGN3+ cells are islet progenitors and are distinct from duct progenitors. *Development* **129**, 2447-2457 (2002).

78. E. L. Jackson *et al.*, Analysis of lung tumor initiation and progression using conditional expression of oncogenic K-ras. *Genes Dev* **15**, 3243-3248 (2001).

79. K. P. Olive *et al.*, Mutant p53 gain of function in two mouse models of Li-Fraumeni syndrome. *Cell* **119**, 847-860 (2004).

80. H. Luche, O. Weber, T. Nageswara Rao, C. Blum, H. J. Fehling, Faithful activation of an extra-bright red fluorescent protein in "knock-in" Cre-reporter mice ideally suited for lineage tracing studies. *Eur J Immunol* **37**, 43-53 (2007).

81. J. Schindelin *et al.*, Fiji: an open-source platform for biological-image analysis. *Nat Methods* **9**, 676-682 (2012).

82. M. Assi, N. Dauguet, P. Jacquemin, DIE-RNA: A Reproducible Strategy for the Digestion of Normal and Injured Pancreas, Isolation of Pancreatic Cells from Genetically Engineered Mouse Models and Extraction of High Quality RNA. *Front Physiol* **9**, 129 (2018).

Figure legends

Figure 1: Cells expressing p53R172H are eliminated from adult pancreas *in vivo*. Co-expression of p53R172H mutations prevents KrasG12D cell elimination *in vivo*.

A Schematic of mouse models (left), tamoxifen treatment and timepoints (right). 6–8-week-old *Pdx1-Cre^{ERT}; Rosa26$^{LSL\text{-}tdRFP}$* (Control), *Pdx1-Cre^{ERT}; Rosa26$^{LSL\text{-}tdRFP}$; LSL-Kras$^{G12D/+}$* (KC), *Pdx1-Cre^{ERT}; Rosa26$^{LSL\text{-}tdRFP}$; LSL-TP53$^{R172H/+}$* (PC), and *Pdx1-Cre^{ERT}; Rosa26$^{LSL\text{-}tdRFP}$; LSL-Kras$^{G12D/+}$; LSL-TP53$^{R172H/+}$* (KPC) mice were treated with one single low dose of tamoxifen. Pancreata were harvested at 7-, 35- or 70-days post tamoxifen induction. Illustration created with BioRender.com. **B** Representative images of endogenous RFP fluorescence showing the area occupied by RFP in Control, KrasG12D (KC), p53R172H (PC) or double mutant (KPC) pancreas tissue sections harvested at 7- days (top) and 35-days (bottom) p.i. Scale bar, 500µm. **C** Percentage of RFP fluorescence per total tissue area from Control, KrasG12D (KC), p53R172H (PC) or double mutant (KPC) tissues at 7- (squares), 35- (circles) and 70-days (triangles) p.i. Each data point represents average RFP fluorescence per mouse; control n=6 (7-days p.i.), n=5 (35-days p.i.), n=4 (70-days p.i.); KC n=6 (7- and 70-days p.i.), n=4 (35-days p.i.); PC n=6 (7-days p.i.), n=5 (35- and 70-days p.i.); KPC n=6 (7-days p.i.), n=4 (35- and 70-days p.i.). The data represent mean and +/- s.d. Student's t test was used to analyse the data, ****p*<0.0001, **p*=0.0173, ns>0.1504. **D** Percentage of RFP+ ducts at 7-days p.i. Ducts that carried at least one RFP+ cell were quantified as positive. Data points represent mean RFP+ percentage per mouse (n=3 per group), with at least 20 ducts counted per mouse. The data represent mean and +/- s.d. Student's t test was used to analyse the data, ***p*<0.004, ns=0.2879. **E** Percentage of RFP+ cells per total number of cells in islets at 35 days p.i. Data represent mean +/- s.d. for at least 23 islets for each genotype from three mice per genotype. Student's t test was used to analyse the data, **p*<0.03, ns=0.5394. **F** Percentage of RFP positive clusters grouped according to cluster area (µm^2). RFP positive cluster area was measured, and clusters were grouped according to their size in 4 groups at 7 and 35 days p.i.: 20-50 µm^2, 51-100 µm^2, 101-1000 µm^2 and more than 1000 µm^2. The graph shows the percentage of clusters in each group relative to the total number of clusters. At 35 days p.i. the percentage of 20-50 µm^2 clusters significantly decreases in KC (*p*=0.0004) and PC (*p*=0.0316), no significant differences were observed in Control or KPC tissues (p=0.7740). Student's t test was used to analyse the data. The data represent mean +/- s.d. for at least 700 clusters were quantified per mouse and 3 mice per genotype/timepoint.

Figure 2: Bulk RNA sequencing results indicate cell fate changes in p53R172H and KrasG12D mutant retained cells.

A Experimental design for tissue collection for RNA sequencing. Control, KC, PC and KPC mice were treated with low dose tamoxifen induction. RFP+ cells were isolated from pancreas tissues harvested at 35 days p.i. for bulk RNA sequencing. Three samples were analysed per genotype, each sample was obtained by pooling the pancreas from three mice. Illustration created with BioRender.com. **B-C** Normalised enrichment scores (NES) of gene set enrichment analysis (GSEA) on the Hallmark and KEGG MEDICUS gene sets for the RNA-seq analysis of **B** KC retained cells or **C** PC retained cells. Only gene sets with an FDR of less than 0.25 were included in the graph. The complete list that contains the results of GSEA analysis is provided in supplementary tables S4-S7.

Figure 3: Cell dormancy/diapause gene signatures and cell cycle arrest are features of non-eliminated Ras mutant cells.

A Percentage of Ki-67 positive cells/total cells in Control, KrasG12D (KC), p53R172H (PC) or double mutant (KPC) pancreas tissues harvested at 7 and 35 days p.i. The data represent mean and +/- s.d. per mouse; control n=6 (7-days p.i.), n=5 (35-days p.i.); KC n=6 (7- and 35-days p.i.); PC n=3 (7- and 35-days p.i.); KPC n=3 (7-days p.i.), n=4 (35- days p.i.) micce. Heatmaps showing row z-scores representing expression of **B** cell cycle associated and **D** cell dormancy (rows) in non-eliminated KrasG12D (KC), non-eliminated p53R172H (PC) or Control cells (columns). Only genes with z-scores of a foldchange of 0.5 for KC average values are shown in Cell cycle panel. The full list of genes can be found in supplementary table S10. **C** Percentage of cleaved caspase-3 positive cells/total cells in Control, KrasG12D (KC), p53R172H (PC) or double mutant (KPC) pancreas tissues harvested at 7 and 35 days p.i. mean +/- s.d. per mouse; control n=5 (7-days p.i.), n=4 (35-days p.i.); KC n=5 (7- and 35-days p.i.); PC n=3 (7-days p.i.), n=6 (35-days p.i.); KPC n=3 (7-days p.i.), n=4 (35- days p.i.) mice. **E** Confocal images of GFP-RasV12 cells-expressing scrambled siRNA (siScr) or two siRNA oligos targeting endogenous *Myc* (siMyc1+2) and then mixed with non-labelled MDCK cells (1:50). Cells were stained with phalloidin to visualise F-actin (red) and Hoechst (blue). Merged images are shown. Scale bar, 100µm. **F** The proportion of non-extruded GFP-RasV12 cells transiently expressing different siRNA *Myc* oligos (siMyc1, siMyc2, siMyc1+2) relative to non-extruded GFP-RasV12 cells expressing siRNA scrambled (siScr). Data represent mean +/- s.d. from three independent experiments. At least 300 cells per point (100 cells per experiment). Student's t test was used to analyse the data, ***$p<0.0005$, *$p<0.05$. **G** Confocal images of GFP-RasV12-expressing siRNA oligos targeting endogenous Myc (siMyc1+2), mixed with non-labelled MDCK cells (1:50). Cells were stained with anti-Ki-67 antibodies (red) and Hoechst (blue). Scale bar, 50 µm. **H** Percentage of Ki-67 positive cells extruded GFP-RasV12 cells as a fraction of total extruded cells. Non-extruded cells

were not Ki-67 positive. Data represent mean +/- s.d. for 60 cells from three independent experiments. Student's t test was used to analyse the data, **p<0.005.

Figure 4: Wnt pathway is activated at normal-mutant cell-cell boundaries *in vivo*.
Heatmaps of **A** Wnt signalling pathway or **B** Wnt/β-catenin pathway related genes (rows) in Control and KrasG12D (KC) cell transcriptomes (columns). The heatmaps show row z-scores for each gene obtained from the RNA sequencing experiment. Data from three samples (three mice pooled per sample) per genotype are shown. Only genes with z-scores of a foldchange of 2 are shown in the Wnt pathway panel. The full list of genes can be found in supplementary table S11. **C** *Wnt5a* mRNA reads relative to control reads in the three samples in Control and three samples in KrasG12D (KC) obtained from the RNA sequencing experiment. Graph represents mean +/- s.d. reads. **D** Confocal images of pancreas tissues harvested at 35-days p.i. from Control, KrasG12D (KC) mice. Tissues were stained with anti-RFP (red) and anti-β-catenin (cyan) antibodies and Hoechst (blue). Dashed boxes represent digital zoom images of representative cell-cell contacts. Scale bar, 50µm. **E** Mean fluorescence intensity of β-catenin at the boundary between RFP positive and negative cells in Control and KrasG12D (KC) tissues harvested at 35 days p.i. Mean fluorescence intensity is relative to the background. Fluorescence was measured in ROIs, separated by a constant distance, along the cell-cell boundary. SuperPlot shows all the quantified ROIs (circles) and the mean for each mouse (n=3 samples; triangle, square and diamond). The graph shows mean and +/- s.d. for the three mice. Student's t test was used to analyse the data. *p=0.0347. **F** Mean fluorescence intensity of β-catenin in the nuclei of RFP positive cells in Control and KrasG12D (KC) tissues harvested at 35 days p.i. Mean fluorescence intensity is relative to the background. SuperPlot shows all the quantified nuclei (circles) and the mean for each mouse (n=3 samples; triangle, square and diamond). The graph shows mean and +/- s.d. for the three mice. Student's t test was used to analyse the data. ns=0.3035. **G** Confocal images of pancreas tissues harvested at 35-days p.i. from Control, KrasG12D (KC) and KrasG12D high dose tamoxifen (KC megadose) mice and stained with anti-RFP (red) and anti-CD44 (cyan) antibodies and Hoechst (blue). Scale bar, 50µm. **H** Mean fluorescence intensity of CD44 at the boundary between RFP positive and RFP negative cells in Control, KrasG12D low dose tamoxifen (KC) and KrasG12D high dose tamoxifen (KC Megadose) tissues harvested at 35 days p.i. CD44 fluorescence was quantified and reported as in F. SuperPlot shows all the quantified ROIs (circles) and the mean for each mouse (n=3 samples; triangle, square and diamond). The graph shows mean and +/- s.d. for the three mice. Student's t test was used to analyse the data. **p=0.0047; ***p=0.0009; ns=0.2136. **I** Mean fluorescence intensity of CD44 in entire RFP positive clusters. Mean fluorescence intensity is relative to the background. SuperPlot shows all the quantified clusters (circles)

and the mean for each mouse (n=3 samples; triangle, square and diamond). The graph shows mean and +/- s.d. for the three mice. Student's t test was used to analyse the data. *p<0.05; ns=0.3916.

Figure 5: Wnt signalling prevents apical extrusion of RasV12 cells from normal epithelial monolayer *in vitro*. Inhibition of Wnt promotes elimination of non-eliminated cells *in vivo.*

A Confocal images of extruded and non-extruded siScr-GFP-RasV12 and siMyc 1+2-GFP-RasV12 cells for 48h with DMSO or WNT-974. Fixed cells were stained with Hoechst (blue). Scale bar, 100 µm. **B** The proportion of non-extruded GFP-RasV12 cells transiently expressing siRNA *Myc* oligos (siMyc1+2) relative to non-extruded GFP-RasV12 cells expressing siRNA scrambled (siScr). Cells were treated with DMSO (white bars) or WNT-974 porcupine inhibitor (dashed bars). The data represent mean +/- s.d. for at least 300 cells from three independent repeats. Student's t test was used to analyse the data. ***p<0.0005. **C** Confocal images of extruded and non-extruded GFP-RasV12 cells pre-treated with PBS/Wnt5a and treated for 48h with DMSO/WNT-974/OMP-18R5. OMP-18R5 is a Frizzled receptor antagonist. Fixed cells were stained with Hoechst (blue). Scale bar, 100 µm. **D, E.** GFP-RasV12 non-extruded cells pre-treated with PBS or Wnt5a recombinant protein 24h before mixing with MDCK cells (1:50). Six hours after mixing and plating, cells were treated with **D** DMSO or WNT-974 porcupine inhibitor or **E** OMP-18R5. The data represent mean +/- s.d. for at least 300 cells from three independent repeats. Student's t test was used to analyse the data, ***p<0.0005, **p<0.005, *p<0.05. **F** Experimental design for Wnt inhibition experiments *in vivo*. 6–8-week-old KC (*Kras*$^{G12D/+}$) mice were induced with low-dose tamoxifen. Thirty-five days later, mice were treated with the porcupine inhibitor WNT-974 or vehicle for 28 days. Illustration created with BioRender.com. **G** Representative images of endogenous RFP fluorescence in KC pancreas tissue sections harvested 28-days post treatment with vehicle or WNT-974. Scale bar, 500µm. **H** RFP fluorescence per tissue area in KC mice treated with WNT-974 or vehicle and relative to vehicle treated tissues. Data represent mean per mouse (n=4-6 samples) and +/- s.d. Student's t test was used to analyse the data, ***p=0.0003.

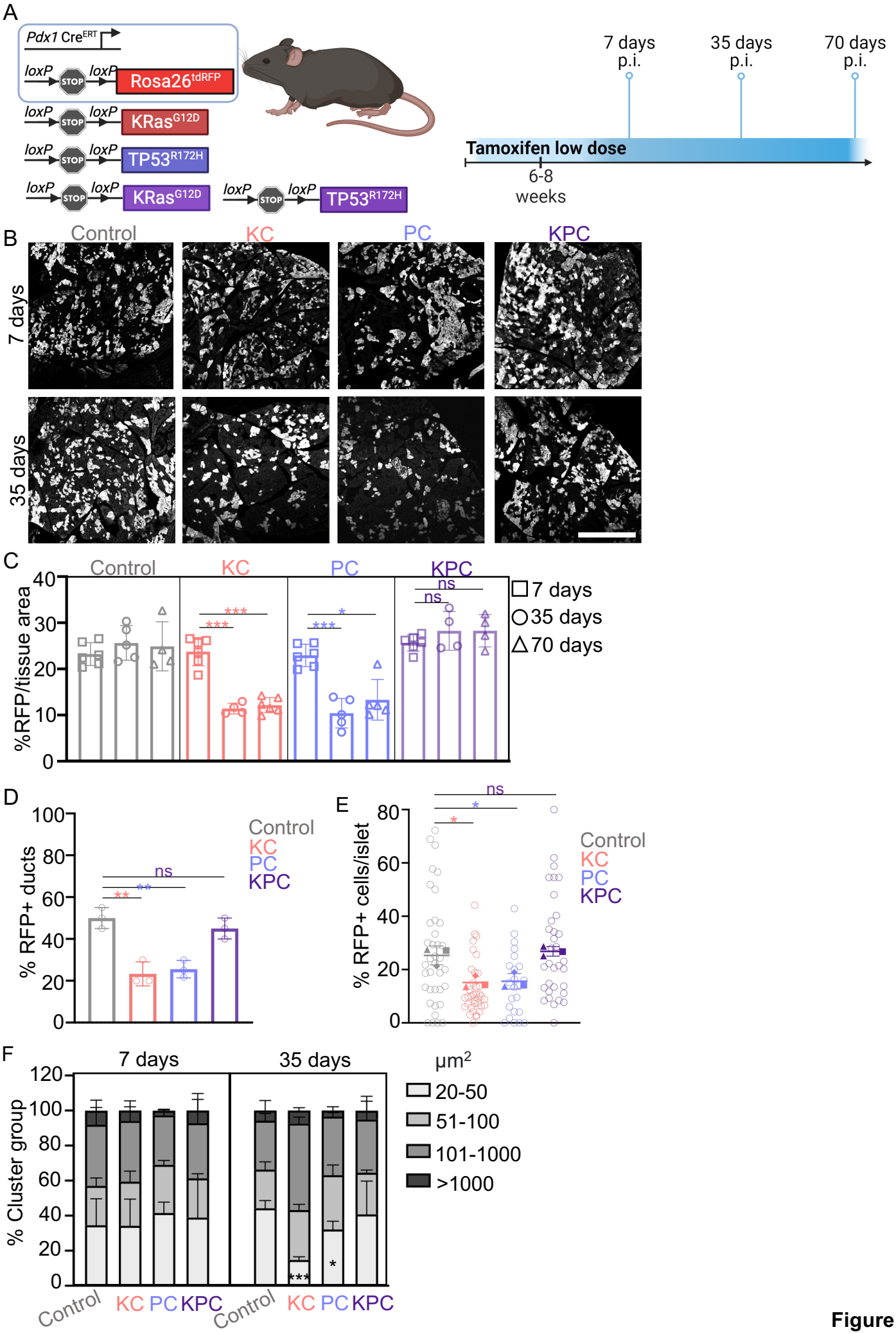
A
Pdx1 Cre^ERT
loxP STOP loxP Rosa26^tdRFP
loxP STOP loxP KRas^G12D
loxP STOP loxP TP53^R172H
loxP STOP loxP KRas^G12D
loxP STOP loxP TP53^R172H
7 days p.i.
35 days p.i.
70 days p.i.
Tamoxifen low dose
6-8 weeks
B
Control
KC
PC
KPC
7 days
35 days
C
%RFP/tissue area
7 days
35 days
70 days
D
% RFP+ ducts
Control
KC
PC
KPC
E
% RFP+ cells/islet
F
% Cluster group
7 days
35 days
μm²
20-50
51-100
101-1000
>1000

Figure 1

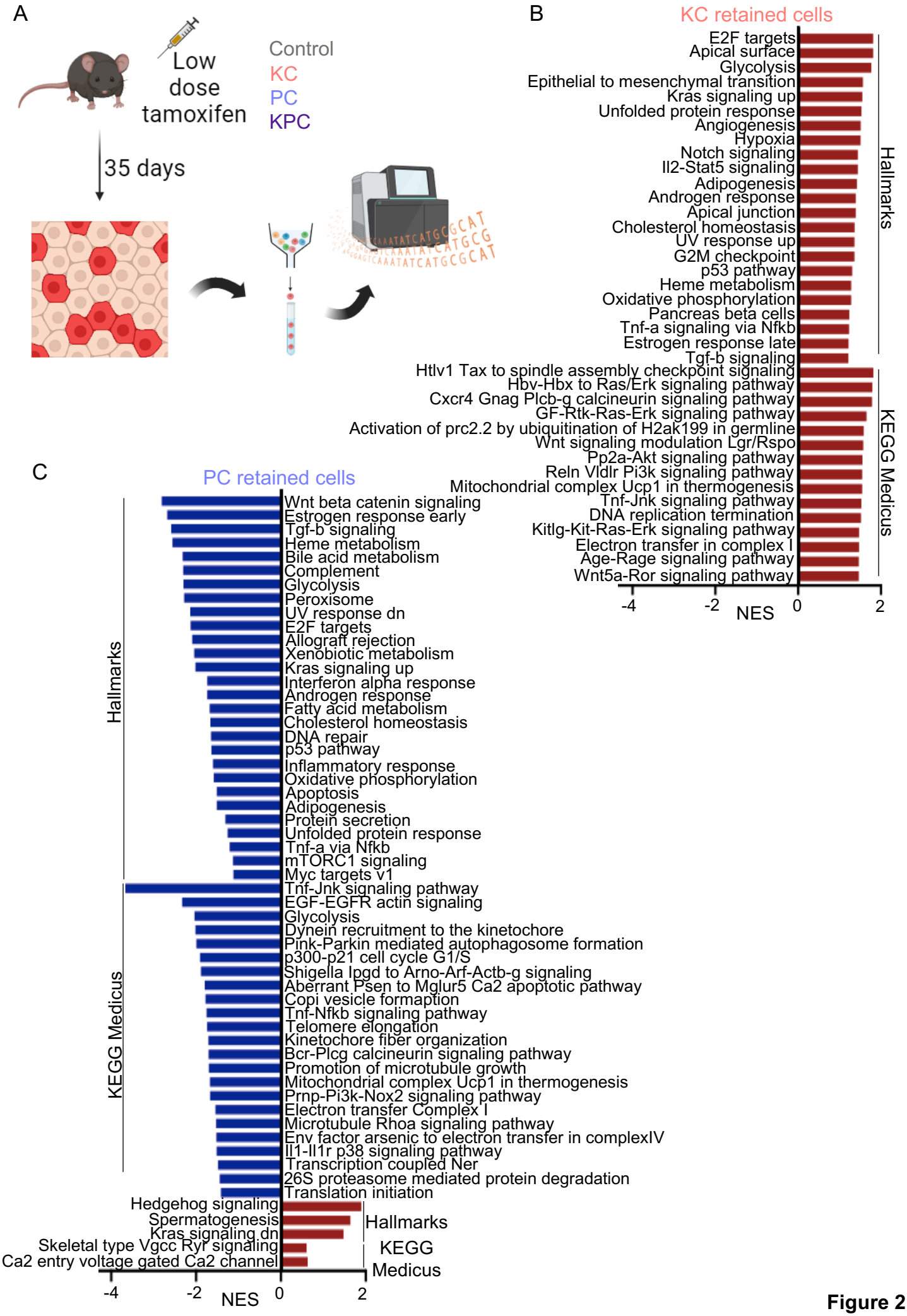
A
Low dose tamoxifen
Control
KC
PC
KPC
35 days
B
KC retained cells
E2F targets
Apical surface
Glycolysis
Epithelial to mesenchymal transition
Kras signaling up
Unfolded protein response
Angiogenesis
Hypoxia
Notch signaling
Il2-Stat5 signaling
Adipogenesis
Androgen response
Apical junction
Cholesterol homeostasis
UV response up
G2M checkpoint
p53 pathway
Heme metabolism
Oxidative phosphorylation
Pancreas beta cells
Tnf-a signaling via Nfkb
Estrogen response late
Tgf-b signaling
Htlv1 Tax to spindle assembly checkpoint signaling
Hbv-Hbx to Ras/Erk signaling pathway
Cxcr4 Gnag Plcb-g calcineurin signaling pathway
GF-Rtk-Ras-Erk signaling pathway
Activation of prc2.2 by ubiquitination of H2ak199 in germline
Wnt signaling modulation Lgr/Rspo
Pp2a-Akt signaling pathway
Reln Vldlr Pi3k signaling pathway
Mitochondrial complex Ucp1 in thermogenesis
Tnf-Jnk signaling pathway
DNA replication termination
Kitlg-Kit-Ras-Erk signaling pathway
Electron transfer in complex I
Age-Rage signaling pathway
Wnt5a-Ror signaling pathway
Hallmarks
KEGG Medicus
-4
-2
NES
0
2
C
PC retained cells
Wnt beta catenin signaling
Estrogen response early
Tgf-b signaling
Heme metabolism
Bile acid metabolism
Complement
Glycolysis
Peroxisome
UV response dn
E2F targets
Allograft rejection
Xenobiotic metabolism
Kras signaling up
Interferon alpha response
Androgen response
Fatty acid metabolism
Cholesterol homeostasis
DNA repair
p53 pathway
Inflammatory response
Oxidative phosphorylation
Apoptosis
Adipogenesis
Protein secretion
Unfolded protein response
Tnf-a via Nfkb
mTORC1 signaling
Myc targets v1
Tnf-Jnk signaling pathway
EGF-EGFR actin signaling
Glycolysis
Dynein recruitment to the kinetochore
Pink-Parkin mediated autophagosome formation
p300-p21 cell cycle G1/S
Shigella Ipgd to Arno-Arf-Actb-g signaling
Aberrant Psen to Mglur5 Ca2 apoptotic pathway
Copi vesicle formaption
Tnf-Nfkb signaling pathway
Telomere elongation
Kinetochore fiber organization
Bcr-Plcg calcineurin signaling pathway
Promotion of microtubule growth
Mitochondrial complex Ucp1 in thermogenesis
Prnp-Pi3k-Nox2 signaling pathway
Electron transfer Complex I
Microtubule Rhoa signaling pathway
Env factor arsenic to electron transfer in complexIV
Il1-Il1r p38 signaling pathway
Transcription coupled Ner
26S proteasome mediated protein degradation
Translation initiation
Hedgehog signaling
Spermatogenesis
Kras signaling dn
Skeletal type Vgcc Ryr signaling
Ca2 entry voltage gated Ca2 channel
Hallmarks
KEGG Medicus
-4
-2
NES
0
2

Figure 2

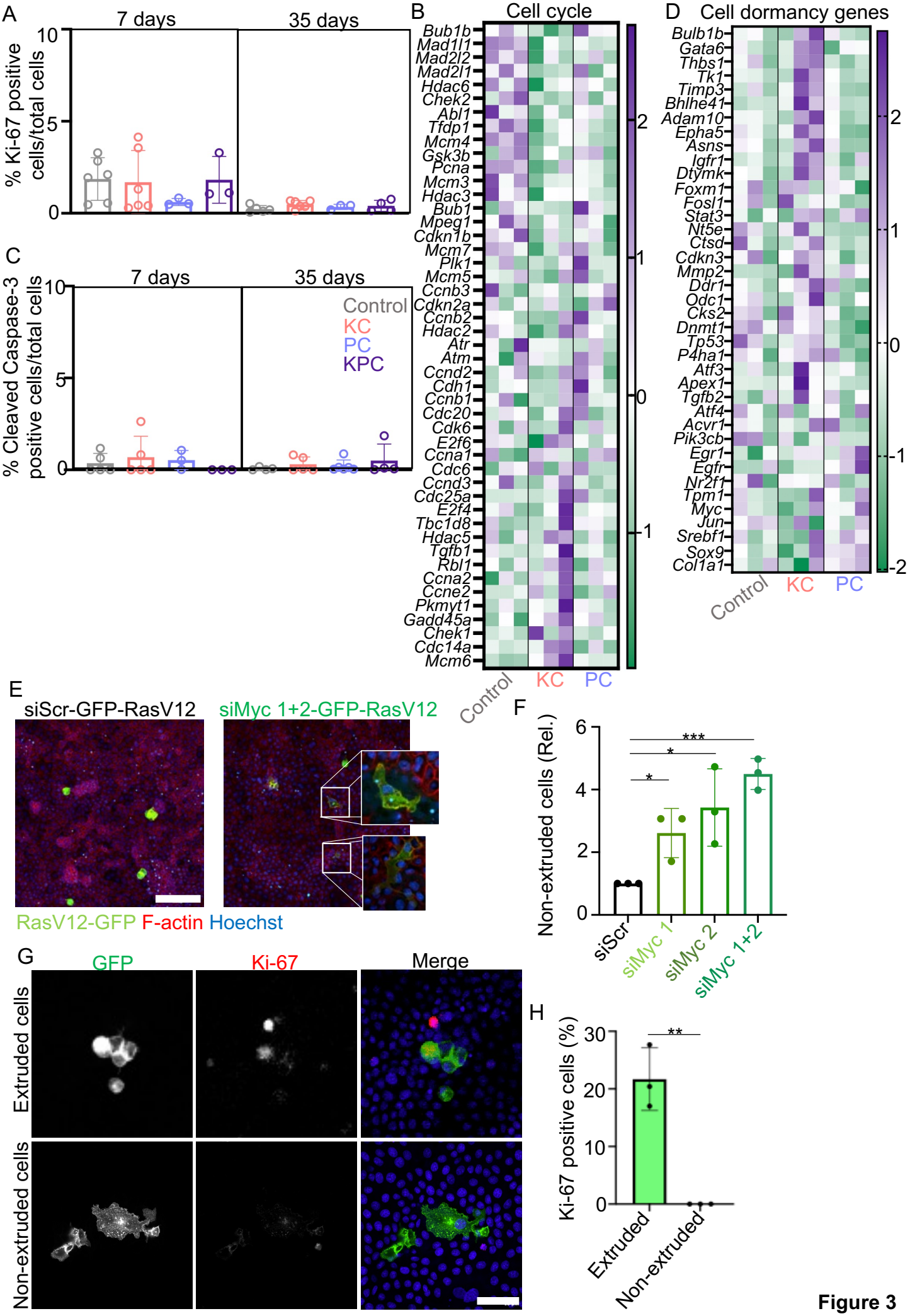
A
7 days
35 days
% Ki-67 positive cells/total cells
10
5
0
C
7 days
35 days
% Cleaved Caspase-3 positive cells/total cells
Control
KC
PC
KPC
B
Cell cycle
Bub1b
Mad1l1
Mad2l2
Mad2l1
Hdac6
Chek2
Abl1
Tfdp1
Mcm4
Gsk3b
Pcna
Mcm3
Hdac3
Bub1
Mpeg1
Cdkn1b
Mcm7
Plk1
Mcm5
Ccnb3
Cdkn2a
Ccnb2
Hdac2
Atr
Atm
Ccnd2
Cdh1
Ccnb1
Cdc20
Cdk6
E2f6
Ccna1
Cdc6
Ccnd3
Cdc25a
E2f4
Tbc1d8
Hdac5
Tgfb1
Rbl1
Ccna2
Ccne2
Pkmyt1
Gadd45a
Chek1
Cdc14a
Mcm6
Control
KC
PC
D
Cell dormancy genes
Bulb1b
Gata6
Thbs1
Tk1
Timp3
Bhlhe41
Adam10
Epha5
Asns
Igfr1
Dtymk
Foxm1
Fosl1
Stat3
Nt5e
Ctsd
Cdkn3
Mmp2
Ddr1
Odc1
Cks2
Dnmt1
Tp53
P4ha1
Atf3
Apex1
Tgfb2
Atf4
Acvr1
Pik3cb
Egr1
Egfr
Nr2f1
Tpm1
Myc
Jun
Srebf1
Sox9
Col1a1
Control
KC
PC
E
siScr-GFP-RasV12
siMyc 1+2-GFP-RasV12
RasV12-GFP F-actin Hoechst
F
Non-extruded cells (Rel.)
siScr
siMyc 1
siMyc 2
siMyc 1+2
G
GFP
Ki-67
Merge
Extruded cells
Non-extruded cells
H
Ki-67 positive cells (%)
Extruded
Non-extruded

Figure 3

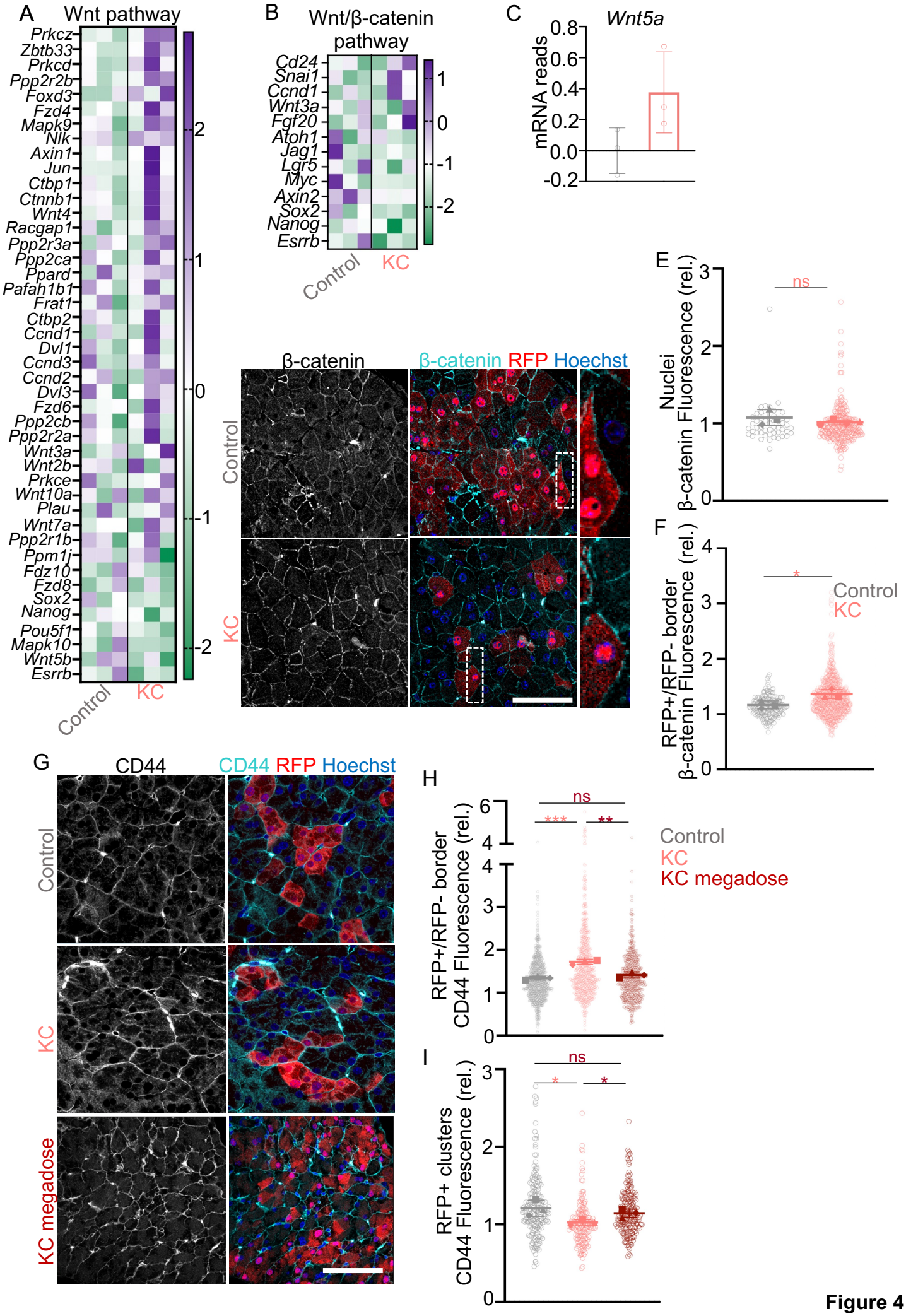
A
Wnt pathway
Prkcz
Zbtb33
Prkcd
Ppp2r2b
Foxd3
Fzd4
Mapk9
Nlk
Axin1
Jun
Ctbp1
Ctnnb1
Wnt4
Racgap1
Ppp2r3a
Ppp2ca
Ppard
Pafah1b1
Frat1
Ctbp2
Ccnd1
Dvl1
Ccnd3
Ccnd2
Dvl3
Fzd6
Ppp2cb
Ppp2r2a
Wnt3a
Wnt2b
Prkce
Wnt10a
Plau
Wnt7a
Ppp2r1b
Ppm1j
Fdz10
Fzd8
Sox2
Nanog
Pou5f1
Mapk10
Wnt5b
Esrrb
Control
KC
2
1
0
-1
-2
B
Wnt/β-catenin pathway
Cd24
Snai1
Ccnd1
Wnt3a
Fgf20
Atoh1
Jag1
Lgr5
Myc
Axin2
Sox2
Nanog
Esrrb
Control
KC
1
0
-1
-2
C
Wnt5a
mRNA reads
0.8
0.6
0.4
0.2
0.0
-0.2
β-catenin
β-catenin RFP Hoechst
Control
KC
E
Nuclei β-catenin Fluorescence (rel.)
ns
F
RFP+/RFP- border β-catenin Fluorescence (rel.)
*
Control
KC
G
CD44
CD44 RFP Hoechst
Control
KC
KC megadose
H
RFP+/RFP- border CD44 Fluorescence (rel.)
ns
***
**
Control
KC
KC megadose
I
RFP+ clusters CD44 Fluorescence (rel.)
ns
*
*

Figure 4

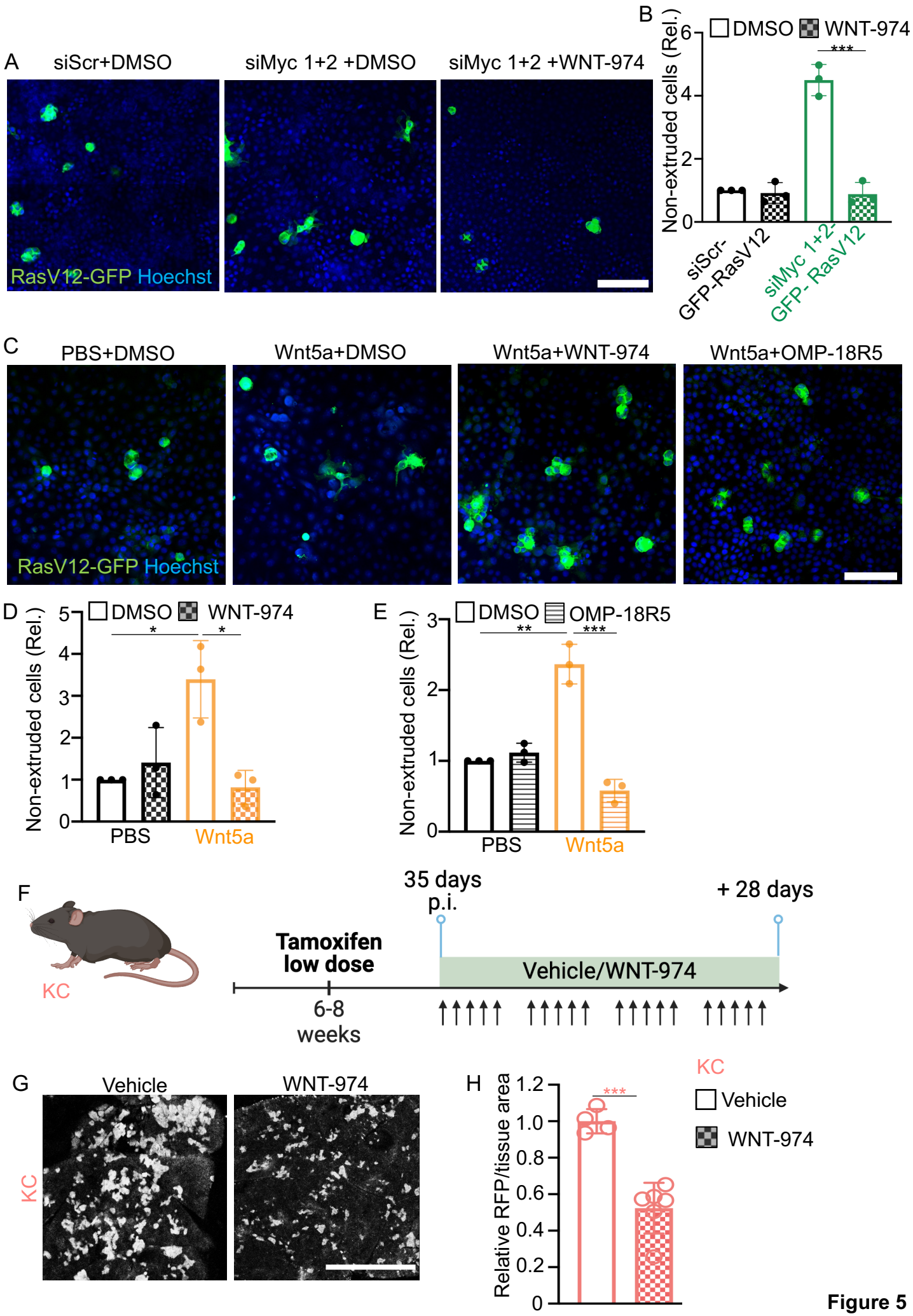
A
siScr+DMSO
siMyc 1+2 +DMSO
siMyc 1+2 +WNT-974
RasV12-GFP Hoechst
B
DMSO
WNT-974
Non-extruded cells (Rel.)
***
siScr-GFP-RasV12
siMyc 1+2-GFP- RasV12
C
PBS+DMSO
Wnt5a+DMSO
Wnt5a+WNT-974
Wnt5a+OMP-18R5
RasV12-GFP Hoechst
D
DMSO
WNT-974
Non-extruded cells (Rel.)
PBS
Wnt5a
E
DMSO
OMP-18R5
Non-extruded cells (Rel.)
PBS
Wnt5a
F
KC
Tamoxifen low dose
6-8 weeks
35 days p.i.
+ 28 days
Vehicle/WNT-974
G
Vehicle
WNT-974
KC
H
KC
Vehicle
WNT-974
Relative RFP/tissue area
***

Figure 5